Analysis of the light intensity dependence of the growth of *Synechocystis* and of the light distribution in a photobioreactor energized by 635 nm light

Alessandro Cordara [1] , **Angela Re** [Corresp., 2] , **Cristina Pagliano** [1] , **Pascal Van Alphen** [3] , **Raffaele Pirone** [4] , **Guido Saracco** [4] , **Filipe Branco dos Santos** [3] , **Klaas Hellingwerf** [3] , **Nicolò Vasile** [2]

[1] Applied Science and Technology Department- Biosolar Lab, Politecnico di Torino, Turin, Italy

[2] Centre for Sustainable Future Technologies, Istituto Italiano di Tecnologia, Turin, Italy

[3] Swammerdam Institute for Life Sciences, University of Amsterdam, Amsterdam, Netherlands

[4] Applied Science and Technology Department, Polytechnic Institute of Turin, Turin, Italy

Corresponding Author: Angela Re
Email address: angela.re@iit.it

Synechocystis gathered momentum in modelling studies and biotechnological applications owing to multiple factors like fast growth, ability to fix carbon dioxide into valuable products, and the relative ease of genetic manipulation. *Synechocystis* physiology and metabolism, and consequently, the productivity of *Synechocystis*-based photobioreactors, are heavily light modulated. Here, we set up a turbidostat-controlled lab-scale cultivation system in order to study the influence of varying orange-red light intensities on *Synechocystis* growth characteristics and photosynthetic activity. *Synechocystis* growth and photosynthetic activity were found to raise as supplied light intensity increased up to 500 µmol photons m^{-2} s^{-1} and to enter the photoinhibition state only at 800 µmol photons $m^{-2}s^{-1}$. Interestingly, reverting the light to a non-photo-inhibiting intensity unveiled *Synechocystis* to be able to promptly recover. Furthermore, our characterization displayed a clear correlation between variations in growth rate and cell size, extending a phenomenon previously observed in other cyanobacteria. Further, we applied a modelling approach to simulate the effects produced by varying the incident light intensity on its local distribution within the photobioreactor vessel. Our model simulations suggested that the photosynthetic activity of *Synechocystis* could be enhanced by finely regulating the intensity of the light incident on the photobioreactor in order to prevent cells from experiencing light-induced stress and induce their exploitation of areas of different local light intensity formed in the vessel. In the latter case, the heterogeneous distribution of the local light intensity would allow *Synechocystis* for an optimized usage of light.

1 **Title: Analysis of the light intensity dependence of the growth of *Synechocystis* and of**

2 **the light distribution in a photobioreactor energized by 635 nm light**

4 **Authors names and affiliations**

5 **Alessandro Cordara[1], Angela Re[2*], Cristina Pagliano[1], Pascal van Alphen[4], Raffaele**

6 **Pirone[3], Guido Saracco[2,3], Filipe Branco dos Santos[4], Klaas J. Hellingwerf[4], Nicolò**

7 **Vasile[2]**

9 **(1) Applied Science and Technology Department - BioSolar Lab, Politecnico di Torino,**

10 **Environment Park.**

11 **(2) Centre for Sustainable Future Technologies, Istituto Italiano di Tecnologia.**

12 **(3) Applied Science and Technology Department, Politecnico di Torino.**

13 **(4) Molecular Microbial Physiology Group, Swammerdam Institute for Life Sciences,**

14 **University of Amsterdam.**

17 **(*) Corresponding author**

19 E-mail: Angela.Re@iit.it

28   **Abstract**

29   *Synechocystis* gathered momentum in modelling studies and biotechnological

30   applications owing to multiple factors like fast growth, ability to fix carbon dioxide into

31   valuable products, and the relative ease of genetic manipulation. *Synechocystis*

32   physiology and metabolism, and consequently, the productivity of *Synechocystis* -based

33   photobioreactors, are heavily light modulated. Here, we set up a turbidostat-controlled

34   lab-scale cultivation system in order to study the influence of varying orange-red light

35   intensities on *Synechocystis* growth characteristics and photosynthetic activity.

36   *Synechocystis* growth and photosynthetic activity were found to raise as supplied light

37   intensity increased up to 500 μmol photons m^{-2} s^{-1} and to enter the photoinhibition state

38   only at 800 μmol photons $m^{-2}s^{-1}$. Interestingly, reverting the light to a non-photo-

39   inhibiting intensity unveiled *Synechocystis* to be able to promptly recover. Furthermore,

40   our characterization displayed a clear correlation between variations in growth rate

41   and cell size, extending a phenomenon previously observed in other cyanobacteria.

42   Further, we applied a modelling approach to simulate the effects produced by varying

43   the incident light intensity on its local distribution within the photobioreactor vessel.

44   Our model simulations suggested that the photosynthetic activity of *Synechocystis* could

45   be enhanced by finely regulating the intensity of the light incident on the

46   photobioreactor in order to prevent cells from experiencing light-induced stress and

47   induce their exploitation of areas of different local light intensity formed in the vessel.

48   In the latter case, the heterogeneous distribution of the local light intensity would allow

49   *Synechocystis* for an optimized usage of light.

53 **Introduction**

54 *Synechocystis* sp. PCC6803 (hereafter *Synechocystis*) was the first photosynthetic organism

55 to have its genome fully sequenced(Kaneko et al., 1996). A wealth of transcriptomic (Anfelt

56 et al., 2013;Beck et al., 2014;Angermayr et al., 2016), proteomic (Fang et al., 2016) and

57 metabolomic (Yang, Hua & Shimizu, 2002;Yoshikawa et al., 2013), studies allowed to

58 investigate *Synechocystis* regulatory, signalling and metabolic pathways in finer details than

59 in any other cyanobacterium. *Synechocystis* has attracted much interest as model organism in

60 product-oriented industrial biotechnology due to the ability to effortlessly recycle carbon

61 dioxide (CO_2) into valuable fuels and chemicals, the simplicity of its culture conditions, the

62 ease of genetic manipulation and its relatively fast cell growth compared to higher plants

63 (Janssen et al., 2003;Angermayr, Hellingwerf & Teixeira de Mattos, 2009) ,. Genetic

64 engineering of cyanobacteria has demonstrated the opportunity to channel solar energy into

65 the formation of various commodity products (Angermayr, Gorchs Rovira & Hellingwerf,

66 2015;Zhou et al., 2016). In the last decades, *Synechocystis* has served in many genetic

67 engineering studies as biofactory for the production of a variety of products (Yu et al.,

68 2013a;Singh et al., 2017), , such as ethanol (Gao et al., 2012), isobutanol(Varman et al.,

69 2013), lactate (Angermayr, Paszota & Hellingwerf, 2012;Joseph et al.) and

70 polyhydroxyalkanoate (Luengo et al., 2003), which can be widely utilized in biotechnology

71 and industrial fields.

72 The intensive exploitation of this microorganism for industrial uses strongly depends on the

73 choice of optimal growth conditions, main operational parameters including culture density

74 (Esteves-Ferreira et al., 2017; Straka & Rittmann, 2018) , pH (Touloupakis et al., 2016),

75 temperature (Panda et al., 2006), mixing rate and light environment (Touloupakis et al., 2016;

76 Singh et al., 2009a). Even though extensive investigation showed that *Synechocystis*

77   productivity is sensitive to most of the aforementioned operational parameters (Yu et al.,

78   2013; Burrows & Wong, 2009; Nanjo et al., 2010; Chaves, Kirst & Melis, 2015), it is

79   undoubted that productivity is tightly coupled with the light absorption efficiency of optical

80   energy conversion systems. Therefore, light management during *Synechocystis* cultivation in

81   photobioreactors (PBRs) is by far the most remarkable factor to account for in order to boost

82   the practical exploitation of this microorganism. *Synechocystis* is able to absorb energy across

83   the visible spectrum, mainly through three classes of pigments: bilins (Gan & Bryant, 2015),

84   chlorophyll *a* (Chl *a*), which is associated with Photosystem II (PSII) and Photosystem I

85   (PSI) reaction centre cores (Vermaas, 1996), and carotenoids (Glazer, 1977; Colyer et al.,

86   2005). Achieving high performance in PBRs requires high intensity light, which nonetheless

87   can cause light associated damages. A number of studies sought to dilute the supplied light

88   intensity by optimizing the light spectra distribution. These attempts were encouraged by the

89   integration of light emitting diodes (LEDs) within indoor PBRs (Ooms et al., 2017). Tailoring

90   light wavelength spectrum affords improved growth conditions stability and reproducibility

91   and has been shown to lead to concrete achievements in biomass productivity and ultimately

92   in the accumulation of useful products. For example, a perfect fit of the red light with the

93   absorption peak of the Chl *a* and phycocyanobilin was observed to lead to an increased

94   growth in cyanobacteria during cultivation (Wyman & Fay, 1986; Wang, Fu & Liu, 2007;

95   Pcc & Alphen, 2018). In other cases, dynamic adjustments of light wavelength during

96   cultivation of *Chlorella vulgaris* and *Haematococcus pluvialis* allowed to increase the

97   microorganism productivity (Katsuda et al., 2004).

98   It is well known that the exposure of photosynthetic organisms to strong solar irradiation

99   results in inhibition of the electron transfer activity of PSII, referred to as photoinhibition

100 responses (Powles, 1984). This phenomenon derives from an imbalance between the

101 photodamage brought to PSII and the repair mechanisms for such damage(Murata et al.,

102   2007). Despite the numerous studies conducted on this topic highlight that the main target

103   of photoinhibition is the D1 protein of PSII reaction centre (Tyystjärvi, 2013), the

104   molecular mechanisms of PSII photoinhibition are not yet completely understood. Upon

105   exposure of photosynthetic organisms to strong irradiation, two mechanisms contribute to the

106   photodamage of PSII, which are called acceptor-side and donor-side photoinhibition. In the

107   acceptor-side mechanism, strong illumination causes the over-reduction of PSII, due to the

108   double reduction of the primary quinone acceptor (Q_A) that, in such condition, can no longer

109   serve as an electron carrier. The recombination between the doubled reduced form of Q_A and

110   the primary radical pair $P680^+$ and $Pheo^-$ leads to the formation of the triplet state of the

111   P680, which can react with molecular oxygen leading to generation of the reactive form of

112   oxygen (ROS) singlet oxygen ($^1O_2$) (Mulo et al., 1998; Vass et al., 1992b). Due to the

113   extremely short lifetime of this ROS, $^1O_2$ is thought to impair mainly the proteins and lipids

114   nearby its production site (Triantaphylidès & Havaux, 2009). Conversely, the donor-side

115   photoinhibition is not mediated by ROS and occurs when the reduction of the PSII is slower

116   than its oxidation, due to inactivation of the oxygen evolving system. This leads to an

117   extended lifetime of the radicals $TyrZ^+$ and $P680^+$ that act as strong oxidants against the

118   surrounding proteins and lipids, resulting in a damage to the PSII(Bumann & Oesterhelt,

119   1995).

120   In this work, we investigated the effect of increasing intensities (in the range 50-1460 µmol

121   photons m^{-2} s^{-1}) of orange-red light on the autotrophic growth of *Synechocystis* in a

122   turbidostat-controlled lab scale PBR. Monitoring *Synechocystis* physiological state under

123   varying light regimes, we found that growth rate, cell size and PSII activity were influenced

124   by light intensity, albeit in slightly different ways. *Synechocystis* cells proved to be resilient

125   to high light stress conditions, suffering photoinhibition only above 800 µmol photons m^{-2} s^{-1},

126   and showed a remarkable ability to recover from the complete state of photoinhibition

127   experienced at 1460 μmol photons m^{-2} s^{-1} when reverting light to 200 μmol photons m^{-2} s^{-1}.

128   Further, we combined the experimental analyses with system modelling and the related multi-

129   physics analysis to investigate the influence of local light intensity distribution on

130   photoinhibition of microorganism.

131   **Materials and methods**

132   **Strain and preculture conditions**

133   For all experiments, we used wild-type *Synechocysti*s sp. PCC 6803, a glucose-tolerant

134   derivative kindly provided by Devaki Bhaya (Department of Plant Biology, Carnegie

135   Institution for Science, Stanford, California, USA). The cells were grown in flasks in 25 ml

136   of BG11 medium (Stanier et al., 1971) with a modified protocol as described in (Van Alphen

137   & Hellingwerf, 2015). Precultures were grown for 4 days at 30˚C in a shaking incubator at

138   120 rpm (New Brunswick Innova 44) under constant illumination of orange-red (632 nm) and

139   blue (451 nm) light (10:1 photon ratio) at 30 μmol photons m^{-2} s^{-1}, measured with a LI-250

140   quantum sensor (LI-COR, USA).

141   **PBR growth conditions**

142   A *Synechocystis* preculture was used to seed the PBR. The culture was grown in a flat panel

143   PBR model FMT150.2/400 Photon System Instruments (Nedbal et al., 2008) in a final

144   volume of approximately 380 ml in the BG-11 medium modified as described above,

145   supplemented with 10 mM of $NaHCO_3$.

146   The PBR (**Fig. 1**) is provided with a combined pH/temperature probe, a Clark-type dissolved

147   O_2 (dO_2) probe (all probes Mattler-Toledo), and an integrated densitometer that measures the

148   optical density (OD) at 720 and 680 nm.

149   The cyanobacterial suspension was illuminated from one side with orange-red light (636 nm)

150   by high-power LEDs. The light regimes applied by the LED board provided cells with the

151   following light intensities as measured outside the PBR, opposite of and at the centre of the

152   light panel: 50, 200, 300, 500, 800, 950 and 1460 µmol photons m^{-2} s^{-1}. The cells were

153   subjected to increasing light intensity every 24 h. The 24 h period of light acclimation was

154   sufficient for establishing stable (variance < 1%) growth rate and dissolved oxygen in the

155   culture medium for each light intensity except for the light regime of 1460 µmol photons m^{-2}

156   s^{-1}, where stable values were not obtained. The temperature and pH were kept constant at

157   30˚C and 8.0, respectively, by automatically adjusting pCO_2 using a gas mixing system

158   GMS150 (Photon Systems Instruments). CO_2 was provided in a mixture with N_2 with a gas

159   flow of 150 ml min^{-1} controlled by a mass flow controller (Smart Mass Flow Model 5850S,

160   Brooks Instruments). The PBR was run in turbidostat mode with the OD_{720}, measured by the

161   integrated densitometer, calibrated to the bench-top spectrophotometer OD_{730} to maintain the

162   OD_{730} at approximately 0.4 (turbidostat set to a maximum deviation of 3%) at 50 µmol

163   photons m^{-2} s^{-1}. The turbidostat mode allowed the culture to hold cell density constant and to

164   remain in exponential phase under all tested light conditions. Dissolved molecular oxygen

165   was normalized to the values obtained at 50 µmol photons m^{-2} s^{-1}.

166

167

168   **Dry weight, cell size and count measurements**

169   At the end of each 24 h step of light increment, 22 ml of culture were harvested to perform in

170   parallel dry weight measurements and cell size analysis.

171   For the determination of dry cell weight, cellulose acetate membranes (0.2 µm, Whatman)

172   were washed with milli-Q water (Merck Millipore Reference), left to dry for 24 h at 90˚C in a

173   stove (Electrolux) and weighted with an analytical balance (AB204, Mettler Toledo).

174   Subsequently, the membranes were used for filtering 20 ml of sampled culture. After washing

175   once with milli-Q water to remove salts, the membrane filter was left to dry overnight in the

176   stove at 90˚C and finally weighted again. In parallel, the OD_{730} of the sampled cells was

177   measured with a spectrophotometer (Lightwave II, Biochrom) and used to normalize the dry

178   cell weight per OD_{730}.

179   The average cell size and cell number were measured with the CASY counter instrument

180   (Roche Applied Science). A volume of 20 µl of harvested culture was diluted with 10 ml of

181   CASY ton solution. The average cell size was measured working in a range of calibration

182   between 0-5 µm with a capillary of 60 µm.

183

184   **Model description**

185   The 3D multi-physics model of the PBR was developed on the COMSOL 5.3® platform and

186   allowed us to simulate different phenomena such as fluid dynamic, light transmission in

187   different media, cyanobacterial growth kinetics and mass transfer by formulating the

188   corresponding equations. **Fig. 1D** shows the design of the 3D model based on the reactor

189   geometry. Free tetrahedral meshing was applied to the created model prior to analysis.

190   Meshing size was selected in order to prevent inaccuracy and imprecision of modelling

191   resulting from model meshing.

192

193   **Assumptions, inlet and boundary conditions**

194   To solve the different mass balances and kinetic equations, it is necessary either to state the

195   initial and boundary conditions, which include inlet, outlet and wall conditions, or to discuss

196   the different assumptions, which clarify the limitations of the created model:

197   i.   the inlet velocity of recycling gas was measured experimentally. As there is no liquid

198   exchanging during experiments, the liquid velocity in the inlet/outlet area is equal to

199   0;

200   ii.   the mass transfer between liquid culture and gas is considered;

201   iii.   all conditions in the model of the PBR, where both liquid and gas phases are present,

202   were formulated by assuming the gas flux at the reactor boundaries negligible and by

203   setting the liquid velocity at the reactor surface wall different from zero. Slip

204   conditions were applied to all PBR walls;

205   iv.   since only CO_2/N_2 gas mixture flows through the sparger, its fluid-dynamic model

206   assumed a single phase to be present. Therefore, the wall conditions used for gas flow

207   were slip conditions, which assume that the gas velocity at the sparger solid surface is

208   calculated by the mathematical model;

209   v.   the working conditions have to be furnished to the model: temperature, inlet gas

210   velocity (or flow rate), initial, inlet and outlet pressure, amount of initial

211   microorganisms and nutrients;

212   vi.   the influence of nutrient concentration, temperature and light intensity on

213   cyanobacterial growth rate are all considered.

214

215   **Mathematical model**

216   The mathematical model is described in the following sections. All the variables and

217   parameters employed in the equations are listed and described in the Nomenclature as well as

218   in Table S1. To estimate the necessary parameters, we relied on experimentally determined

219   values or on an inference procedure by fitting model simulations to observed data.

220   Specifically, we compared simulated and experimental data using a statistical analysis of

221   errors based on the Levenberg-Marquardt method, coupled with the second least-squares

222   analysis. Since the method implements a constrained search procedure, it requires specifying

223   lower and upper bounds on the unknown parameters, which were selected within the ranges

224   of values most frequently observed in literature. The parameter space exploration stopped

225   when the model simulation best fit the experimental data.

226   **Fluid-dynamic equations**

227   We generally need to model different domains inside the bioreactor: a gas-liquid mixture

228   inside the vessel, and a single gas phase inside the sparger domain. Therefore, the continuity

229   equations and the momentum balance equations need to be adapted depending on the

230   modelled domain.

231

232   The general double-phase fluid dynamic continuity equations are formulated through Eqs. (1-

233   3) and allow to account for the coexistence of the bubble gas phase (dispersed phase, named

234   by "d" as subscript) and the liquid phase (continuous phase, named by "c" as subscript):

235

236    $(\rho_c - \rho_d)\left[\nabla \cdot \left(\Phi_d(1 - c_d)\mathbf{u}_{slip} - D_{md}\nabla \cdot \Phi_d\right) + \frac{m_{dc}}{\rho_d}\right] + \rho_c(\nabla \cdot \mathbf{u}) = 0$ (1)

237

238    $\mathbf{u} = \dfrac{\phi_c\rho_c\mathbf{u}_c + \phi_d\rho_d\mathbf{u}_d}{\rho}$ (2)

239

240    $\emptyset_c + \emptyset_d = 1$ (3)

241

242   where **Eq. (1)** is the continuity equation, **Eq. (2)** expresses the velocity vector u, Φc

243   and Φd are the volume fractions corresponding to liquid and gas phases respectively, and ρ

244   is the pseudo-continuous phase density. **Eq. (3)** describes the relation between the volume

245   fractions for the continuous Φc and dispersed Φd phases.

246
247   As to the sparger, since a single gas phase exists, we modelled the fluid dynamic variables

248   trends accounting only for the terms of the **(Eq. 1)** related to the gas phase, which is

249   expressed by the following equation:

250 $\frac{\partial \rho_g}{\partial t} + \nabla \cdot (\rho u)_g = 0$ (4)

251

252 Regarding the momentum balance equations, we adopted the Navier–Stokes model for the

253 liquid–gas multiphase system, by using the following formulation (Li, Hu & Liu, 2014)

254 $\frac{\partial (\rho \mathbf{u})}{\partial t} + \nabla \cdot (\rho \mathbf{uu}) = -\nabla p - \nabla \cdot \boldsymbol{\tau} + \rho \mathbf{g} + \mathbf{F}$ (5)

255

256 $\boldsymbol{\tau} = -\mu \left[(\nabla \mathbf{u} + (\nabla \mathbf{u})^{\mathrm{T}}) - \frac{2}{3} (\nabla \cdot \mathbf{u})\mathbf{I} \right]$ (6)

257

258 where p is the pressure, g is the gravity acceleration vector, $\boldsymbol{\tau}$ is the stress tensor and μ is the

259 effective viscosity. For the single-phase sparger model, the momentum balance equations are

260 similar to **Eq.(5)**, where we replaced the effective viscosity with the gas viscosity.

261 In **Eq.(5)**, the effective viscosity includes not only the molecular viscosity μ_i but also

262 turbulent viscosity $\mu_{i,T}$ (Luo & Al-Dahhan, 2011), which accounts for the influence exerted by

263 the turbulent flow**Eq.(7)**.

264 Among the several models introduced to handle the turbulent viscosity, we adopted the

265 standard k-ε model to simulate the turbulent flow of the fluid entrained with cyanobacteria in

266 the mechanically stirred PBR. The standard k–ε turbulent model is computationally stable,

267 even in the presence of complex physics, and is applicable to a wide variety of turbulent

268 flows.

269 The equations to calculate the effective viscosity within the k–ε model are listed below:

270

271 $\mu_{eff} = \mu_i + \mu_{i,T}$ (7)

272 $\mu_{\mathrm{T}} = \rho C_\mu \frac{k^2}{\varepsilon}$ (8)

273

274 where $C\mu$ is a model constant equals to 0.09 and k is the turbulence kinetic energy which can

275 be calculated by the transport equations (Ali, 2014)

276

277 $$\rho \frac{\partial k}{\partial t} + \rho \mathbf{u} \cdot \nabla k = \nabla \cdot \left(\left(\mu + \frac{\mu_T}{\sigma_k} \right) \nabla k \right) + \mathbf{P}_k - \rho \varepsilon \qquad (9)$$

278

279 Where σ_k is a model constant equals to 1.0, derived from (Wilcox, 2006). To obtain the P_k

280 values we used **Eq.(10)**

281

282 $$\mathbf{P}_k = \mu_T \left(\nabla \mathbf{u} \left(\nabla \mathbf{u} + (\nabla \mathbf{u})^\mathrm{T} \right) - \frac{2}{3} (\nabla \cdot \mathbf{u})^2 \right) - \frac{2}{3} \rho k \nabla \cdot \mathbf{u} \qquad (10)$$

283

284 where the value of turbulent energy dissipation rate ε was calculated by **Eq.(11)**:

285

286 $$\rho \frac{\partial \varepsilon}{\partial t} + \rho \mathbf{u} \cdot \nabla \varepsilon = \nabla \cdot \left(\left(\mu + \frac{\mu_T}{\sigma_\varepsilon} \right) \nabla \varepsilon \right) + C_{\varepsilon 1} \frac{\varepsilon}{k} \mathbf{P}_k - C_{\varepsilon 2} \rho \frac{\varepsilon^2}{k} \qquad (11)$$

287

288 In this equation, $C_{\varepsilon 1}$ and $C_{\varepsilon 2}$ are constants equal to 1.44 and 1.92, respectively. Finally, in a

289 turbulent bubbly flow model, the difference between gas velocity and liquid velocity consists

290 of two terms: slip velocity and drift velocity (**Eq. (12)**):

291

292 $$\mathbf{u}_d - \mathbf{u}_c = \mathbf{u}_{slip} - \frac{D_{md}}{(1-c_d)\Phi_d} \qquad (12)$$

293

294 The slip velocity $\boldsymbol{u}_{slip}$ represents the relative velocity of the phases and the drift velocity is the

295 additional velocity appearing when turbulence is taken into account. The drift velocity can be

296 calculated by **Eq.(13)**, whereas the slip velocity can be calculated by using a pressure–drag

297 balance (**Eq.(14)**):

299 $$u_{drift} = -\frac{D_{md}}{(1-c_d)}\nabla\emptyset_d \qquad (13)$$

300

301 $$\frac{3C_{drag}}{4d_b}|u_{slip}|u_{slip}\rho_l = -\nabla p \qquad (14)$$

302

303 where the drag coefficient C_{drag} can be computed by different formulas (Hartmann et al.,

304 2013). In our case, C_d was computed by **Eq.(15)**:

305

306 $$C_d = \frac{0.622}{\frac{\xi}{g\rho_l d_b^2}+0.235} \qquad (15)$$

307

308 where ζ is the surface tension coefficient and d_b is the average bubble diameter which was

309 measured as 3 mm through video imaging (d_b = 3 mm).

310 **Heat transfer with radiation: light transmission equations**

311 The balance of the radiative intensity, including contributions regarding propagation,

312 emission, absorption and scattering is formulated through the general radiative transfer

313 equation (Modest, 2003) and can be written as follows:

314
315 $$\Omega \cdot \nabla I(\Omega) = \kappa I_b(T) - \beta I(\Omega) + \frac{\sigma_S}{4\pi}\int_{4\pi} I(\Omega')\Phi(\Omega',\Omega)d\Omega' \qquad (16)$$
316
317 To account for the effect mediated by the bubble volume fraction and cyanobacterial cell

318 concentration, we adapted the Lambert-Beer's law:

319
320 $$\frac{I}{I_0} = exp\,(-\beta z) \qquad (17)$$
321
322 where I is the local light intensity and I_0 represents the incident light intensity, β is the

323 extinction coefficient and z represents the path-length of the light through the material. Eq.

324 (17) does not account either for the light scattering by bubbles, which change the direction of

325 light transmission, either for the light absorption by cyanobacteria [51]. Therefore, we

326 modified Eq. 17 as follows:

327 $\frac{I}{I_0} = exp\left(-\left(\frac{\beta S}{4} + K_a\right)z\right)$ (18)

328

329 **Eq. (18)** accounts for light absorption by *Synechocystis* cells by means of kα, which is the

330 absorption coefficient associated with cyanobacteria, and for the scattering associated with

331 the bubble volume fraction through *S*, the interfacial area per unit volume which is a function

332 of bubble size and bubble number density. By replacing the interfacial area with the bubble

333 volume fraction $\emptyset_d$ and the bubble diameter, d_b, **Eq. (18)** is converted in the equation **Eq.**

334 **(19)**:

335

336 $\frac{I}{I_0} = exp\left(-\frac{3\emptyset_d z}{d_b} - K_a z\right)$ (19)

337 The difference between **Eq. (17)** and **Eq. (19)** is the effect of cyanobacteria light absorption

338 on local light intensity distribution. The average diameter of bubbles was calculated by using

339 the video imaging technique and performing the procedure described in (Ali, 2014; Zhang,

340 Dechatiwongse & Hellgardt, 2015). **Eq. (19)** was then used in the general radiative transfer

341 equation.

342 Calculating the radiative heat source requires information on the temperature regime

343 throughout the entire vessel domain, which is obtained solving the general heat transfer

344 balance equation. The general heat transfer balance (Bird, Stewart & Lightfoot, 2002), which

345 takes into account the radiation in participating media, is expressed in **Eq.(20)**

346

347 $\rho C_p \frac{\partial T}{\partial t} + \rho C_p \mathbf{u} \cdot \nabla T + \nabla \cdot \mathbf{q} = Q + Q_r$ (20)

348

349   where Q_r is the radiative heat source expressed as **Eq.(21)**

350

351   $Q_r = \kappa(G - 4\pi I_b)$ (21)

352

353   **Kinetic models and calculation theory: cyanobacterial growth equations**

354   Generally, cyanobacterial growth rate is strongly influenced by various factors such as

355   temperature, light intensity and nutrient concentration. Temperature usually affects the

356   activity of enzymes involved in the cellular duplication, whereas light intensity determines

357   the energy that cells can absorb for their maintenance and growth. Nutrient elements

358   including sulphur, carbon, phosphorus and nitrogen are necessary for cyanobacteria to

359   compose their biomass (Dechatiwongse et al., 2014).

360   The kinetics of cyanobacterial growth is usually defined by the Monod model, **Eq.(22)**,

361   which only considers the effect of nutrient concentration (Vatcheva et al., 2006), because

362   additional environmental parameters such as temperature and light intensity are always kept

363   constant during experiments (Solimeno et al., 2015). In the Monod model, as shown in

364   **Eq.(22)**, the maximum specific growth rate μ_{max} is treated as a constant, but in reality it is a

365   function of light intensity and temperature. When nutrients are in excess, the growth rate is

366   independent of nutrient concentration and expressed as:

367

368   $\mu_{gr} = \mu_{max}\dfrac{C}{k_s+C}$

369   (22)

370

371   where C is the concentration of the limiting substrate for growth. In order to take into account

372   also the effects exerted by nutrients and local light intensity on cyanobacterial growth

373   kinetics, we decided to evaluate a modified Monod equation: the Aiba model (Aiba, 1982).

374   The Alba model, shown in **Eq.(23)**, is usually employed to simulate the effect of light

375   intensity on cyanobacterial growth rate: it is capable of modelling the photo-limitation regime

376   under low light intensity, the photo-saturation regime under optimal light intensity, and the

377   photo-inhibition regime under intense light intensity (Zhang et al., 2015). Similarly, the

378   model can also be applied to describe the photo-dependence of the oxygen production rate.

379   In this equation,

380    $$\mu_{gr} = \frac{\mu_{max} \cdot I}{I + k_s + \frac{I^2}{k_i}} \tag{23}$$

381   μ_{max} is the maximum growth rate, and k_s and k_i refer to the light saturation and photo-

382   inhibition, respectively. These parameters are only dependent on cyanobacterial properties

383   and were fitted from experimental observations.

384   All the variables and parameters used in the mathematical models are listed and explained in

385   the nomenclature and in Table S1of Supporting Information.

386

387   **Determination of the photosynthetic efficiency**

388   The photosynthetic efficiency was calculated as grams of biomass formed per mol photons.

389   We calculated the amount of light available to the culture as the input to the PBR, which we

390   called I_{in}, minus the light remaining after the passage through the culture, which we called

391   I_{out}. I_{out} was calculated through model simulations to calculate how much light was absorbed

392   in the reactor volume in 1 hour. We used the growth rate and dry weight values to calculate

393   how much biomass was produced in these square centimetres times the 2.4 cm depth of the

394   culture for the actual volume in one hour.

395

396

397   **Results**

Growth rate, oxygen evolution activity and dimension of cells are dynamically regulated by light intensity

During cultivation, orange-red light was used since it resulted in an optimal light regime for growing *Synechocystis* in our PBRs system. Conversely, light with wavelengths lower than 580 nm (green-blue) or higher than 670 nm (far-red) proved to be not efficient for its growth (Singh et al., 2009). This knowledge served as a prerequisite to set up experiments aiming to quantitatively evaluate the effects of increasing intensities, ranging between 50-1460 μmol photons m^{-2} s^{-1}, of red-orange light on the adjustments of the physiological state in *Synechocystis*. We studied the long-term photoinhibition in *Synechocystis* grown at increasing light intensities by analysing changes in the growth rate, the physiological parameter of oxygen evolution activity and the cell size at each incremental step of light intensity. By running the PBR in turbidostat mode, *Synechocystis* was grown in a semi-continuous regime so that cells were constantly maintained in the exponential growth phase.

Firstly, we measured *Synechocystis* growth rate to evaluate its generation time, and the amount of oxygen dissolved in the medium (dO_2), which provides an indication of the PSII activity within cell (Schuurmans et al., 2015). Both the growth rate of *Synechocystis* (**Fig. 2A)** and the dissolved oxygen produced by the cells (**Fig. 2B**) were clearly affected by increasing light intensity. The dynamics of both variables could be broadly partitioned into four phases: an initial phase at 50 μmol photons m^{-2} s^{-1} where cells were not photoinhibited, a second phase up to 500 μmol photons m^{-2} s^{-1}, where *Synechocystis* cells doubling time and PSII activity attained their maximum values, a third photoinhibitory phase up to 1460 μmol photons m^{-2} s^{-1} where both parameters dropped off, and a final recovery phase at 200 μmol photons m^{-2} s^{-1}. Hereafter, the photon irradiance of 50 μmol photons m^{-2} s^{-1}, was considered the control photon irradiance. At this light condition, cells featured a relatively slow metabolism, as evidenced by the modest growth rate of 0.054 ± 0.003 h^{-1} (corresponding to a

423 doubling time of ≈ 13 h) and a limited level of oxygen dissolved in the medium (roughly 35

424 µM). This dissolved oxygen concentration at this photon irradiance was used as reference to

425 normalize the measurements at all sampled points (normalized reference value at one). At a

426 photon irradiance of 200 µmol photons m^{-2} s^{-1} *Synechocystis* grew two times faster than in the

427 control light condition, showing a growth rate of 0.114 ± 0.005 h^{-1} (corresponding to a

428 doubling time of ≈ 6 h), as shown in **Fig. 2A**. When photon irradiance was increased up to

429 300 and 500 µmol photons m^{-2} s^{-1}, the growth rate remained constant yielding values of 0.117

430 ± 0.006 h^{-1} and 0.114 ± 0.005 h^{-1}, respectively. Switching photon irradiance from 50 to 200

431 µmol photons m^{-2} s^{-1} led to a higher than two-fold increase in the relative amount of oxygen

432 dissolved in the medium (from 1.00 ± 0.02 to 2.22 ± 0.07, as shown in **Fig. 2B**), similarly to

433 the trend displayed by growth rate. However, differently from the *Synechocystis* growth rate,

434 when we increased photon irradiance to 300 µmol photons m^{-2} s^{-1}, the relative concentration

435 of oxygen kept increasing up to 2.56 ± 0.12. Such difference in growth rate and dO$_2$ within

436 the photon irradiance range from 200 and 300 µmol photons m^{-2} s^{-1} suggests that light could

437 exert different effects on the PSII functionality and the doubling time of the microorganism.

438 In particular, the increase in dO$_2$ concentration measured in the cultivation medium could

439 indicate a fine tuning of the light/energy conversion by PSII, whereas the unvaried growth

440 rate observed could result from a limited utilization of the light energy absorbed (Kramer &

441 Evans, 2011). At a photon irradiance of 800 µmol photons m^{-2} s^{-1} a substantial decrease was

442 observed for both growth rate (0.1 ± 0.012 h^{-1} corresponding to a doubling time of ≈ 7 h) and

443 relative amount of dO$_2$ (2.34 ± 0.11), denoting a light intensity where *Synechocystis* cells

444 started to get photoinhibited. Further increasing the photon irradiance up to 1460 µmol

445 photons m^{-2} s^{-1}, *Synechocystis* growth rate dropped off to 0.043 ± 0.020 h^{-1} (corresponding to

446 a doubling time of ≈ 16 h), representing roughly half of the maximum growth rate observed

447 in our experimental set up. Furthermore, over the 24 hours acclimation period at this extreme

448 light treatment, the growth rate was found to be constantly decreasing thus highlighting a

449 severe state of growth inhibition. Together with the growth rate, the relative dO_2 reached its

450 minimum of 1.45 ± 0.23 at 1460 µmol photons m^{-2} s^{-1}. These results evidenced severe PSII

451 photodamage caused in *Synechocystis* by its exposure to high light intensity, in accordance

452 with extensive literature available for cyanobacteria (see review (Murata et al., 2007) and

453 references therein). To test whether, upon photoinhibition, lowering light intensity could

454 recover the growth rate of *Synechocystis*, a point of recovery was set to the lowest light

455 irradiance at which the maximal growth rate was observed (i.e. 200 µmol photons m^{-2} s^{-1}).

456 Upon reverting the photon irradiance to 200 µmol photons m^{-2} s^{-1}, cells showed a remarkable

457 ability to recover completely from the state of photoinhibition, as attested by the increased

458 growth rate up to 0.102 ± 0.009 h^{-1} (corresponding to a doubling time of ≈ 7 h), which is

459 similar to the maximum growth rate previously measured under the same light condition (**Fig.**

460 **2A** (black dot) and **Fig. 3**). Similarly, the relative concentration of dO_2 in the medium was

461 found to increase up to 2.13 ± 0.24, attesting a full recovery of the PSII activity as well (**Fig.**

462 **2B** (black dot) and **Fig. 3**). We found that the recovery half-time is approximately 3 h and

463 that both growth rate and dO_2 remain stable after recovery during the 24 h.

464 As aforementioned, our phenotypic characterization included *Synechocystis* cell size, which

465 was found to vary across the experimentally tested conditions. Even though the bacterial life

466 cycle is usually the major determinant of morphological traits, including cell size, several

467 studies reported that cyanobacteria modify their morphology to optimize their functionality to

468 exogenous factors in natural contexts (Montgomery, 2015). However, the mechanisms by

469 which light conditions, including light intensity, influence cell morphology, including cell

470 size, are understudied (Pattanaik, Whitaker & Montgomery, 2011). Table 1 shows

471 *Synechocystis* cell size changes in response to increasing light intensities. At 50 µmol

472 photons m^{-2} s^{-1} the cell size was 2.11 ± 0.06 µm. This size is commonly observed in

473 *Synechocystis* cells cultivated under non-stressful conditions (Du et al., 2016). At a photon

474 irradiance of 500 μmol photons m^{-2} s^{-1} *Synechocystis* cells reached the maximum size of 3.29

475 ± 0.13 μm while, at the photon irradiance of 800 μmol photons m^{-2} s^{-1}, which was found to

476 induce photoinhibition, *Synechocystis* cell size decreased to 3.09 ± 0.23 μm and then

477 gradually to 2.69 ± 0.21 μm at the maximal photoinhibitory photon irradiance of 1460 μmol

478 photons m^{-2} s^{-1}. Notably, at the recovery light regime of 200 μmol photons m^{-2} s^{-1},

479 *Synechocystis* cells recovered the dimension previously observed under the control photon

480 irradiance (3.02 ± 0.13 μm). Altogether, cell size, growth rate and PSII functionality behaved

481 similarly under increasing intensities of orange-red light, by reaching their maximal values at

482 intensities up to 500 μmol photons m^{-2} s^{-1} and rapidly decreasing at photoinhibiting light

483 conditions.

484

485 We then examined the effect of long-term acclimation to increasing intensities of orange-red

486 light by estimating the Chl *a* content in *Synechocystis* through the measurement of the

487 OD$_{680}$/OD$_{720}$ ratio **(Table S2)**. Our measurements revealed the highest content of Chl *a* at 50

488 μmol photons m^{-2}s^{-1} compared to the other photon irradiances tested **(Table S2)**. These data

489 show that at limited light intensity *Synechocystis* sustains its growth by accumulating a high

490 amount of Chl *a* to maximize light absorption. Increasing the photon irradiance to 200 μmol

491 photons m^{-2}s^{-1}, the amount of Chl *a* decreased by around 13%, which reached the minimum at

492 800 μmol photons^{-2} s^{-1}. Chl *a* reduction could be provoked by its synthesis inhibition in order

493 to limit the absorption of harmfully excessive light(Kada et al., 2003; Xu et al., 2004).

494 Unexpectedly, we observed Chl *a* increased also at 950 and 1460 μmol photons m^{-2}s^{-1}, which

495 were shown to induce severe cell photoinhibition (**Fig. 2**).

496

497 **Influence of local light intensity distribution on photoinibition of microorganism**

498   Our multi-physics analysis focused on the spread of incident light within the *Synechocystis*

499   cultivation apparatus and on the relationships between local light intensity and *Synechocystis*

500   photosynthetic activity, which expectedly influence PBR productivity. The PBR used for

501   culturing *Synechocystis*, the illumination setup and real-time monitoring are extensively

502   described in **Fig. 1**, **Table S3**, **Table S4**and **Fig**. **S1.** The *in silico* simulations have been

503   developed under identical operational conditions as employed during the experiments, and

504   are aimed at exploring the distribution of local light intensity within the cultivation apparatus

505   as a function of the incident light intensity.

506   As thoroughly described in the Methods section, current knowledge on mass transfer, fluid

507   dynamics, heat transfer from radiation, and growth kinetics were entirely incorporated to

508   frame the modelling equations (**Table S1**), and the resulting model was implemented within

509   the COMSOL 5.3® computing platform. To obtain suitable estimates for the parameters

510   necessary to our mathematical representation, we relied either on experimentally determined

511   values or on an inference procedure by fitting model simulations to observed data. The

512   observed agreement between model estimates and experimental measurements for growth

513   rate and dissolved oxygen (**Figs. 2** and **3**) demonstrated that our model is built on solid

514   foundations. Moreover, we employed the light intensities recorded in our model simulations

515   to estimate the light-dependent photosynthetic efficiency of the PBR in terms of moles of

516   photons absorbed in the PBR per gram of biomass production, as shown in **Table 2 and**

517   **Table S5**.

518   The observed agreement between model estimates and experimental measurements for

519   growth rate and dissolved oxygen (**Figs. 2** and **3**) demonstrated that our model is built on

520   solid foundations. Moreover, we employed the light intensities recorded in our model

521   simulations to estimate the light-dependent photosynthetic efficiency of the PBR in terms of

522   moles of photons absorbed in the PBR per gram of biomass production, as shown in **Table 2**.

523 These simulation results fully agree with experimental data acquired in previous studies

524 (Schuurmans et al., 2015), and corroborated the plausibility of our modelling framework. The

525 photosynthetic efficiency of *Synechocystis* turned out to decrease from the highest value,

526 observed at 50 μmol photons m^{-2}s^{-1} where 2.70 g of biomass are produced per mol of

527 photons, to the lowest value observed at 950 μmol photons m^{-2}s^{-1} where 0.48 g of biomass

528 are produced per mol of photons. Moreover, the estimates of photosynthetic efficiency

529 obtained by our model simulations confirmed that efficiency starts to drop fastest in the initial

530 increase in intensity, which is expected at low OD batch cultures. Model simulations were

531 then used to get insights into the local light intensity distribution along different combinations

532 of directional axes within the cultivation apparatus. To ensure comparability of the results

533 shown throughout our analysis, we normalized the light intensity values corresponding to the

534 PBR internal space and resulting from our model simulations with respect to the initial

535 incident intensity on the PBR surface, and we plotted the ratio between the calculated light

536 intensity and the initial incident intensity

$$R_I = \frac{I_{calc}}{I_{inc}}$$

537 To analyse the distribution of light along all the directions, the trends of R_I were developed

538 by the YZ and XZ planes (**Fig. 1D** and **Fig. S2**). The light intensity distribution inside the

539 liquid mixture on six YZ slices for three different incident light intensities, 50, 300 and 950

540 μmol photons m^{-2}s^{-1}, shown in **Fig. 5**, confirms the ability of our modelling approach to

541 capture a number of features of radiation spreading within a cultivation system. Boundary

542 conditions and the coexistence of an upper gas phase and a lower liquid phase are expected to

543 influence the light intensity distribution. Our modelling approach foresaw that the incident

544 light gets reduced where the culture and glass of the vessel interface closest to the side where

545 light is supplied. This reduction amounted to about 3-5%, and was more evident at lower

546 intensities (**Fig. 5**). Moreover, in the area at the interface between the liquid and gas phases

547 light intensity was found to display an eyelet-like pattern where the upper region shows

548 higher intensity than the lower one. Additionally, this pattern was more remarkable for lower

549 values of the incident light intensity. Another source of variation in the spatial distribution of

550 light is identifiable in the rotating domain created by the stirring bar **(Fig. S1)**. The local

551 liquid movement propelled by the stirring bar rotation is expected to favour the light

552 transmission process(Zhang, Dechatiwongse & Hellgardt, 2015). Our model simulations

553 consistently predicted the increase of light intensity in the stirring bar neighbourhood, which

554 amounted to around 3-5% for low I_{inc} and around 1-2% for high I_{inc} **(Fig. 5C)**.

555 In the interface area between the liquid phase and the bottom steel base, our model predicts a

556 reduction in light intensity owing to the large difference between the absorption and

557 emissivity values of these two domains.Beyond these effects, light intensity generally

558 decreased with the distance from the light source, as shown by the plots at equally spaced

559 slices along the YZ axis **(Fig. 5)** and further confirmed by the plots acquired at three XZ

560 sections (**Fig. 6**, **Fig. S2**).

561 The light intensity decay along the path inside the cultivation apparatus was expected since it

562 can be attributed to the compound effect of photon absorption by *Synechocystis* cells and of

563 scattering phenomena (Grima et al., 1994). When varying the incident light intensity, our

564 model simulations showed the extent of light decay to get lower at progressively higher

565 incident light intensity. Decrease in light decay along the path amounting about 18% for I_{inc}

566 of 50 μmol photons m^{-2}s^{-1}, 12% for I_{inc} of 300 μmol photons m^{-2}s^{-1} and 7% for I_{inc} of 950

567 μmol photons m^{-2}s^{-1} were calculated.Our modelling framework was primed to afford the

568 exploration of the relationship between the heterogeneity in local light distribution, which

569 originates from the aforementioned sources, and the *Synechocystis* behaviour in the

570 artificially lit cultivation system. More precisely, we expected the light environment created

571   by the coexistence of regions of higher and lower local light intensity could favour

572   *Synechocystis* functionalities, as gauged by the experimental measurements shown in **Fig. 2**.

573   From our model simulation results, it was evident that at 50 µmol photon $m^{-2}s^{-1}$ the light

574   penetration inside the culture was extremely low **(Fig. 5A)**, suggesting that the cells were

575   exposed to a period of lower intensity considerably longer than the expected light phase set

576   experimentally. Under this light condition *Synechocystis* showed low growth rate, limited

577   amount of oxygen dissolved in the medium (**Fig. 2**), and a higher Chl *a* amount than in the

578   other tested conditions (**Table S1**), which is likely due to the need of optimizing light

579   absorption in a scarcely lit environment. Our simulations showed that, upon increasing the

580   irradiance to 300 µmol photon m^{-2} s^{-1}, light managed to diffuse more deeply within the PBR

581   interior **(Fig. 5B** and **Fig 6)**. The overall increased light availability and the coexistence of

582   regions of different local light intensities created the most favourable light environment for

583   *Synechocystis* which indeed reached its maximal growth rate and oxygen dissolved in the

584   medium (**Fig. 2**). Conversely, the further rise of light intensity up to 950 µmol photons m^{-2} s^{-}

585   ^{1}, and the subsequent suppression of low local light intensity experienced by the cells (**Figs.**

586   **5C** and **6**), led *Synechocystis* to suffer high light stress reflected in a noticeable decrease in its

587   growth rate and oxygen evolution activity (**Fig. 2**). Under such light conditions, cells were no

588   longer able to dissipate the excess of supplied light and entered a photoinhibition state

589   (Chiang, Lee & Chen, 2011).

590

591   **Discussion**

592   The experiments conducted were particularly informative for studying the effects of

593   increasing intensities, ranging between 50-1460 µmol photons m^{-2} s^{-1}, of red-orange light on

594   the adjustments of the physiological state in *Synechocystis*. Although the PSII photodamage

595   effect caused by the exposure to high (white) light intensity is well-established in plants

596 (Theis & Schroda, 2016), corresponding quantitative data on photoinhibition by red light in

597 cyanobacteria are scarce. Furthermore, experimental evidence of the recovery potential in

598 *Synechocystis* from this light stress has so far been lacking. Importantly, our results

599 evidenced the adaptive capacity of *Synechocystis* to completely recover from the harmful

600 condition of photoinhibition under subsequent exposure to an optimal light intensity for

601 growth. It is already well known that under photoinhibitory conditions, loss of oxygen

602 evolution capacity of PSII activates the PSII repair cycle and that the rate of the repair

603 reaction depends on the extent of the PSII damaged centres (Tyystjärvi, 2013). Since the D1

604 protein is the main target of photoinhibition and its lack within the PSII centre speeds up its

605 synthesis, an increase of the amount of psbA transcript in *Synechocystis* occurs in high light

606 (Mohamed et al., 1993) and this high level is maintained for several hours in darkness (He &

607 Vermaas, 1998). Here the quick recovery of PSII activity observed at 200 μmol photons m−2

608 s−1 suggests that the high levels of D1 transcript maintained within the surviving cells at

609 1460 μmol photons m−2 s−1 allows the acceleration of D1 synthesis to reactivate the PSII

610 activity, once cells have been reverted to the optimal growth irradiance. An exceptional

611 capacity to cope with fluctuations in a wide range of lights differing for spectral quality and

612 quantity, as well as pH and temperature, was previously observed in this microorganism by

613 (Constant et al., 2000) and (Zavřel et al., 2015). Indeed, the ability to readily adapt the

614 metabolism to different environmental conditions allowed *Synechocystis*, and more in general

615 cyanobacteria, to proliferate even in extreme environments on Earth (Hernández-Prieto et al.,

616 2016).

617 Furthermore, growth rate was found to positively correlate with cell size independently of

618 light intensity (**Fig. 4**). This trend has been previously observed in *Synechocystis* acclimated

619 to lower intensities of light (Du et al., 2016) and in *Synechococcus* grown under limited

620 nutrient supply of phosphate and nitrate (Garcia, Bonachela & Martiny, 2015), and hints at a

621 light coordination of growth rate with cell size. It has been reported that cyanobacteria can

622 respond to different abiotic stresses by increasing the cell size, accumulating granules of

623 different nature, e.g. glycogen, upon exposure to high light intensity (Kopecna et al., 2012)

624 and polyhydroxybutyrate in case of high temperatures (Červený et al., 2015). Even though

625 the mechanisms that associate cellular growth rate with cell size are still unclear (Amir,

626 2014), here we suggest that the increase of light intensity could accelerate both the

627 metabolism and growth rate of *Synechocystis*, favouring the accumulation of higher amounts

628 of biomass that need to be properly stored, leading the cells to increase their size (Amir,

629 2014; Ferrezuelo et al., 2012). In general, the variation in cell size observed at incremental

630 steps of light intensity was accompanied by the maintenance of a relatively constant dry cell

631 weight per OD730 (Table 1), which suggests that the fluctuations observed in cell size

632 exposed to increasing light intensities were counterbalanced by opposite fluctuations in the

633 number of cells per volume.

634 The highest content of Chl a at 50 μmol photons $m^{-2}s^{-1}$ along with its decrease at increasing

635 orange-red light intensities which we observed upon increasing the orange-red light intensity

636 are expected since inhibition of Chl a synthesis could serve to limit the absorption of

637 harmfully excessive light. Conversely, the Chl a increase observed at 950 and 1460 μmol

638 photons $m^{-2}s^{-1}$, which were shown to induce severe cell photoinhibition (**Fig. 2**), is

639 unexpected. This observation warrants further investigation but it is plausible to hypothesize

640 that the observed increase in Chl *a* amount could be partially due to the accumulation of this

641 pigment in dead cells, which likely reflects the much longer lifetime of Chl molecules with

642 respect to that of other pigments (Steiger, Schäfer & Sandmann, 1999; Vavilin, Brune &

643 Vermaas, 2005; Vavilin & Vermaas, 2007; Yao et al., 2011;Yao, Brune & Vermaas, 2012;

644 Trautmann, Beyer & Al-Babili, 2013; Havaux, 2014). Finally, the recovery of pigment

645 biosynthesis observed upon acclimation of photoinhibited cells over 24 h at 200 μmol

646 photons m^{-2}s^{-1} confirmed the elevated degree of plasticity of this cyanobacterium to cope

647 with extremely high light intensities.

648 The *in silico* simulations were focused to investigate the spatial distribution of local light

649 intensity in the cultivation system on the basis of the incident light intensity and the . Our

650 model simulation allowed a careful, albeit qualitative, evaluation of the complex

651 consequences that variations in light intensity and local light distribution can cause on the

652 *Synechocystis* physiology within an artificially lit cultivation system. In particular, we were

653 able to identify three distinct operative states: i) a light limited state where all the light

654 supplied to the system is maximally exploited by the cells, a condition that is reflected in a

655 linear relation between irradiance and *Synechocystis* physiological parameters, ii) a light

656 optimal state where *Synechocystis* optimizes the utilization of light to support its maximal

657 growth rate and photosynthetic activity, iii) a photo-inhibition state where the excess of

658 incident light becomes harmful for microorganisms growth. Our model simulations suggest

659 that regulating the incident light on the PBR, at least in a range of moderate intensities, could

660 be used to enhance *Synechocystis* growth. Indeed, this model takes into account the formation

661 of areas of different local light intensity within the PBR, whose extent varies as a function of

662 the incident light intensity, and that can be exploited by the microorganism to prevent from

663 experiencing light-induced stress. According to our study, managing local light effects is

664 expected to be worth careful consideration in PBR design for leveraging the microorganism

665 exploitation.

666

667 **Conclusions**

668 The productivity of PBRs exploiting *Synechocystis* clearly depends on the photosynthetic

669 efficiency of this microorganism. Since this efficiency largely depends on the cyanobacteria

670 ability to manage the light collected in the cultivation apparatus, in this work we thoroughly

671 investigated the impact of the setup of the light conditions in the PBR on *Synechocystis*

672 growth and photosynthetic activity. Monitoring *Synechocystis* physiological state under

673 increasing intensities of orange-red light, we found that growth rate, cell size and PSII

674 activity were influenced by light intensity, although in slightly different ways. *Synechocystis*

675 cells proved to be resistant to high light stress conditions, showing photoinhibition only

676 above 800 µmol photons m^{-2} s^{-1} combined with a remarkable ability to recover from the

677 complete state of photoinhibition experienced at 1460 µmol photons m^{-2} s^{-1} when reverting

678 light to 200 µmol photons m^{-2} s^{-1}. Considering the notable plasticity of *Synechocystis* in

679 response to changes in light intensity, we searched for unknown features of the PBR light

680 conditions that could leverage *Synechocystis* behavioural features to enhance the overall PBR

681 productivity. To this end, we deemed it particularly useful to adopt also an *in silico*

682 methodology by constructing a PBR model and subsequently use it to simulate the effects of

683 increasing incident light intensities on the local light intensity distribution. Interestingly, our

684 results indicate that the formation of areas of different light intensities could be controllable

685 by tuning the incident light intensity on the PBR. A gain in *Synechocystis* viability is

686 achievable by increasing the incident light intensity as far as areas of different local light

687 intensities exist to allow *Synechocystis* cells to escape from the photoinhibition state. It is

688 useful to note that the observations herein presented are drawn from experiments and

689 simulations carried out in turbidostat mode (constant OD_{730}) and could vary depending on the

690 choice of the cultivation mode. Nonetheless, our results provide useful insights in a PBR

691 modelling perspective and, in particular, suggest that a PBR design would benefit from

692 considering the management of local light heterogeneity to increase the microorganism

693 photosynthetic activity, by limiting photoinhibition phenomena, to ultimately maximize the

694 productivity.

695

...

696 **Author contributions**

697 Conceived and designed the experiments: Pascal van Alphen, Klaas J Hellingwerf. Performed

698 the biological experiments: Alessandro Cordara. Performed the modelling experiments:

699 Nicolò Vasile. Analyzed the data: Pascal van Alphen, Cristina Pagliano, Klaas J Hellingwerf,

700 Angela Re. Contributed reagents/materials/analysis tools: Pascal van Alphen, Klaas J

701 Hellingwerf, Guido Saracco. Wrote the paper: Alessandro Cordara, Cristina Pagliano, Nicolò

702 Vasile, Angela Re, Pascal van Alphen, Klaas J Hellingwerf. Supervised the study: Filipe

703 Branco dos Santos, Klaas J Hellingwerf, Guido Saracco, Raffaele Pirone.

704

705

706 **Nomenclature**

707 A area, m^2

708 c_d mass fraction of dispersed phase, $kg\ kg^{-1}$

709 C concentration, $mol\ m^{-3}$

710 C_p specific heat at constant pressure, $J\ m^{-3}\ K^{-1}$

711 D diffusion coefficients, $m^2\ s^{-1}$

712 D_{md} turbulent dispersion coefficient, $m^2\ s^{-1}$

713 e enthalpy flux density, $J\ m^{-2}\ s^{-1}$

714 E_A activation energy, $J\ mol^{-1}$

715 F force term, $kg\ m^{-2}\ s^{-2}$

716 G incident light radiation, $W\ m^{-2}$

717 $h_j(T)$ enthalpies heat flux densities, $J\ m^{-2}\ s^{-1}$

718 I incident light intensity, $W\ m^{-2}$

719 I_b black body radiation, Wm^{-2}

720 $\mathbf{J}$ diffusion vector

721 k turbulent kinetic energy, m^2s^{-3}

722 K_r reaction rate constant, $m^2\ s^{-1}$

723 m mass of species, kg

724 m_{dc} mass transfer from dispersed to continuous phase, $kg\ m^{-3}s^{-1}$

725 M molar mass, $kg\ mol^{-1}$

726 n flux density, $mol\ m^{-2}\ s^{-1}$

727 n_d relative mass flux, $mol\ m^{-2}\ s^{-1}$

728 p pressure, Pa

729 q heat flux densities, $W\ m^{-2}$

730 Q volumetric charge density, $C\ m^{-3}$

731 Q_r radiative flux, $W\ m^{-2}$

732 R universal gas constant, $J\ K^{-1}\ mol^{-1}$

733	T	temperature, K
734	u	velocity vector, m s^{-1}
735	u_c	continuous phase velocity vector, m s^{-1}
736	u_d	dispersed phase velocity vector, m s^{-1}
737	u_{slip}	slip velocity vector, m s^{-1}
738	v_p	the convective velocity, m s^{-1}
739	w	volume fraction
740	x	mass fraction
741		

742

Greek symbols

743	β	extinction coefficient , m^{-1}
744	ε	turbulent energy dissipation, m^{2}s^{-3}
745	k_c	effective thermal conductivity coefficient, W m^{-1} K^{-1}
746	κ	absorbance coefficient, m^{-1}
747	μ	dynamic viscosity, kg$_f$ s m^{-2}
748	μ_{gr}	growth rate, h^{-1}
749	μ_T	turbulent viscosity,
750	v	stoichiometric coefficients
751	ρ	density, Kg m^{-3}
752	σ_S	scattering coefficient, m^{-1}
753	τ	turbulent stress,
754	ϕ_c	continuous phase fraction, -
755	ϕ_d	dispersed phase fraction, -
756	ω	rotational velocity, rad s^{-1}

757

758

759 **References**

760 Aiba S. 1982. Growth kinetics of photosynthetic microorganisms. In: Springer, Berlin,

761   Heidelberg, 85–156. DOI: 10.1007/3540116982_3.

762 Ali A. 2014. CFD Simulation of Bubbly Flow Through a Bubble Column. 5:904–910.

763 Amir A. 2014. Cell size regulation in bacteria. *Physical Review Letters* 112:1–5. DOI:

764   10.1103/PhysRevLett.112.208102.

765 Anfelt J., Hallström B., Nielsen J., Uhlén M., Hudson EP. 2013. Using transcriptomics to

766   improve butanol tolerance of *Synechocystis* sp. strain PCC 6803. *Applied and*

767   *environmental microbiology* 79:7419–27. DOI: 10.1128/AEM.02694-13.

768 Angermayr SA., van Alphen P., Hasdemir D., Kramer G., Iqbal M., van Grondelle W.,

769   Hoefsloot HC., Choi YH., Hellingwerf KJ. 2016. Culturing *Synechocystis* sp. Strain

770   PCC 6803 with N2 and CO2 in a Diel Regime Reveals Multiphase Glycogen Dynamics

Alessandro Cordara 6/12/2018 3:18 PM

771   with Low Maintenance Costs. *Applied and environmental microbiology* 82:4180–9.

772   DOI: 10.1128/AEM.00256-16.

773   Angermayr SA., Gorchs Rovira A., Hellingwerf KJ. 2015. Metabolic engineering of

774   cyanobacteria for the synthesis of commodity products. *Trends in Biotechnology*

775   33:352–361. DOI: 10.1016/j.tibtech.2015.03.009.

776   Angermayr SA., Hellingwerf KJ., Teixeira de Mattos MJ. 2009. Energy biotechnology with

777   cyanobacteria. *Current Opinion in Biotechnology* 20:257–263. DOI:

778   10.1016/J.COPBIO.2009.05.011.

779   Angermayr SA., Paszota M., Hellingwerf KJ. 2012. Engineering a cyanobacterial cell factory

780   for production of lactic acid. *Applied and Environmental Microbiology* 78:7098–7106.

781   DOI: 10.1128/AEM.01587-12.

782   Beck C., Hertel S., Rediger A., Lehmann R., Wiegard A., Kölsch A., Heilmann B., Georg J.,

783   Hess WR., Axmann IM. 2014. Daily Expression Pattern of Protein-Encoding Genes and

784   Small Noncoding RNAs in *Synechocystis* sp. Strain PCC 6803. *Applied and*

785   *Environmental Microbiology* 80:5195–5206. DOI: 10.1128/AEM.01086-14.

786   Bird RB (Robert B., Stewart WE., Lightfoot EN. 2002. *Transport phenomena*. J. Wiley.

787   Bumann D., Oesterhelt D. 1995. Destruction of a single chlorophyll is correlated with the

788   photoinhibition of photosystem II with a transiently inactive donor side. *Proceedings of*

789   *the National Academy of Sciences of the United States of America* 92:12195–12199.

790   DOI: 10.1073/pnas.92.26.12195.

791   Burrows EH., Wong W-K., Fern X., Chaplen FWR., Ely RL. 2009. Optimization of pH and

792   nitrogen for enhanced hydrogen production by *Synechocystis* sp. PCC 6803 via

793   statistical and machine learning methods. *Biotechnology Progress* 25:1009–1017. DOI:

794   10.1002/btpr.213.

795   Červený J., Sinetova MA., Zavřel T., Los DA. 2015. Mechanisms of high temperature

796   resistance of *Synechocystis* sp. PCC 6803: An Impact of histidine kinase 34. *Life* 5:676–

797   699. DOI: 10.3390/life5010676.

798   Chaves JE., Kirst H., Melis A. 2015. Isoprene production in *Synechocystis* under alkaline and

799   saline growth conditions. *Journal of Applied Phycology* 27:1089–1097. DOI:

800   10.1007/s10811-014-0395-2.

801   Chiang C-L., Lee C-M., Chen P-C. 2011. Utilization of the cyanobacteria *Anabaena* sp. CH1

802   in biological carbon dioxide mitigation processes. *Bioresource Technology* 102:5400–

803   5405. DOI: 10.1016/j.biortech.2010.10.089.

804   Colyer CL., Klinkade CS., Viskari PJ., Landers JP. 2005. Analysis of cyanobacterial

805   pigments and proteins by electrophoretic and chromatographic methods. *Analytical and*

806   *Bioanalytical Chemistry* 382:559–569. DOI: 10.1007/s00216-004-3020-4.

807   Constant S., Eisenberg-Domovitch Y., Ohad I., Kirilovsky D. 2000. Recovery of

808   photosystem II activity in photoinhibited Synechocystis cells: Light-dependent

809   translation activity is required besides light- independent synthesis of the D1 protein.

810   *Biochemistry* 39:2032–2041. DOI: 10.1021/bi9914154.

811   Dechatiwongse P., Srisamai S., Maitland G., Hellgardt K. 2014. Effects of light and

812   temperature on the photoautotrophic growth and photoinhibition of nitrogen-fixing

813   cyanobacterium *Cyanothece* sp. ATCC 51142. *Algal Research* 5:103–111. DOI:

814   10.1016/J.ALGAL.2014.06.004.

815   Du W., Jongbloets JA., Pineda Hernandez H., Bruggeman FJ., Hellingwerf KJ., Branco dos

816   Santos F. 2016. Photonfluxostat: A method for light-limited batch cultivation of

817   cyanobacteria at different, yet constant, growth rates. *Algal Research* 20:118–125. DOI:

818   10.1016/j.algal.2016.10.004.

819   Esteves-Ferreira AA., Inaba M., Obata T., Fort A., Fleming GTA., Araújo WL., Fernie AR.,

820   Sulpice R. 2017. A Novel Mechanism, Linked to Cell Density, Largely Controls Cell

821   Division in *Synechocystis*. *Plant physiology* 174:2166–2182. DOI:

822   10.1104/pp.17.00729.

823   Fang L., Ge H., Huang X., Liu Y., Lu M., Wang J., Chen W., Xu W., Wang Y. 2016. Trophic

824   Mode-Dependent Proteomic Analysis Reveals Functional Significance of Light-

825   Independent Chlorophyll Synthesis in *Synechocystis* sp. PCC 6803. *Molecular Plant*

826   6803:73–85. DOI: 10.1016/j.molp.2016.08.006.

827   Ferrezuelo F., Colomina N., Palmisano A., Garí E., Gallego C., Csikász-Nagy A., Aldea M.

828   2012. The critical size is set at a single-cell level by growth rate to attain homeostasis

829   and adaptation. *Nature communications* 3:1012. DOI: 10.1038/ncomms2015.

830   Gan F., Bryant DA. 2015. Adaptive and acclimative responses of cyanobacteria to far-red

831   light. *Environmental Microbiology* 17:3450–3465. DOI: 10.1111/1462-2920.12992.

832   Gao Z., Zhao H., Li Z., Tan X., Lu X., Lu X., Foust TD., Hallett JP., Leak DJ., Liotta CL.,

833   Mielenz JR., Murphy R., Templer R., Tschaplinski T. 2012. Photosynthetic production

834   of ethanol from carbon dioxide in genetically engineered cyanobacteria. *Energy*

835   *Environ. Sci.* 5:9857–9865. DOI: 10.1039/C2EE22675H.

836   Garcia NS., Bonachela JA., Martiny AC. 2015. Growth-dependent cell size controls

837   interactions between nutrient supply and cellular elemental stoichiometry of marine

838   *Synechococcus*. *In review*:1–10. DOI: 10.1038/ismej.2016.50.

839 Glazer AN. 1977. Structure and molecular organization of the photosynthetic accessory
840   pigments of cyanobacteria and red algae. *Molecular and Cellular Biochemistry* 18:125–
841   140. DOI: 10.1007/BF00280278.

842 Grima EM., Camacho FG., Pérez JAS., Sevilla JMF., Fernández FGA., Gómez AC. 1994. A
843   mathematical model of microalgal growth in light-limited chemostat culture. *Journal of*
844   *Chemical Technology AND Biotechnology* 61:167–173. DOI: 10.1002/jctb.280610212.

845 Hartmann P., Nikolaou A., Chachuat B., Bernard O., Nikolaou A., Chachuat B. 2013. A
846   dynamic Model coupling Photoacclimation and Photoinhibition in Microalgae *European*
847   *Control Conference*.

848 Havaux M. 2014. Carotenoid oxidation products as stress signals in plants. *The Plant Journal*
849   79:597–606. DOI: 10.1111/tpj.12386.

850 He Q., Vermaas W. 1998. Chlorophyll a availability affects psbA translation and D1
851   precursor processing in vivo in *Synechocystis* sp. PCC 6803. *Proceedings of the*
852   *National Academy of Sciences* 95:5830–5835. DOI: 10.1073/pnas.95.10.5830.

853 Hernández-Prieto M a., Semeniuk TA., Giner-Lamia J., Futschik ME. 2016. The
854   Transcriptional Landscape of the Photosynthetic Model Cyanobacterium *Synechocystis*
855   sp. PCC6803. *Scientific reports* 6:22168. DOI: 10.1038/srep22168.

856 Janssen M., Tramper J., Mur LR., Wijffels RH. 2003. Enclosed outdoor photobioreactors:
857   Light regime, photosynthetic efficiency, scale-up, and future prospects. *Biotechnology*
858   *and Bioengineering* 81:193–210. DOI: 10.1002/bit.10468.

859 Joseph A., Aikawa S., Sasaki K., Tsuge Y., Matsuda F., Tanaka T., Kondo A. 2013.
860   Utilization of Lactic Acid Bacterial Genes in *Synechocystis* sp. PCC 6803 in the
861   Production of Lactic Acid. *Bioscience, Biotechnology, and Biochemistry* 77:966–970.
862   DOI: 10.1271/bbb.120921.

863 Kada S., Koike H., Satoh K., Hase T., Fujita Y. 2003. Arrest of chlorophyll synthesis and
864   differential decrease of Photosystems I and II in a cyanobacterial mutant lacking light-
865   independent protochlorophyllide reductase. *Plant molecular biology* 51:225–35.

866 Kaneko T., Sato S., Kotani H., Tanaka A., Asamizu E., Nakamura Y., Miyajima N.,
867   Hirosawa M., Sugiura M., Sasamoto S., Kimura T., Hosouchi T., Matsuno A., Muraki
868   A., Nakazaki N., Naruo K., Okumura S., Shimpo S., Takeuchi C., Wada T., Watanabe
869   A., Yamada M., Yasuda M., Tabata S. 1996. Sequence analysis of the genome of the
870   unicellular cyanobacterium *Synechocystis* sp. strain PCC6803. II. Sequence
871   determination of the entire genome and assignment of potential protein-coding regions.
872   *DNA research : an international journal for rapid publication of reports on genes and*

873   *genomes* 3:109–36.

874   Katsuda T., Lababpour A., Shimahara K., Katoh S. 2004. Astaxanthin production by

875   *Haematococcus pluvialis* under illumination with LEDs. *Enzyme and Microbial*

876   *Technology* 35:81–86. DOI: 10.1016/J.ENZMICTEC.2004.03.016.

877   Kopecna J., Komenda J., Bucinska L., Sobotka R. 2012. Long-term acclimation of the

878   cyanobacterium *Synechocystis* PCC 6803 to high light is accompanied by an enhanced

879   production of chlorophyll that is preferentially channeled to trimeric PSI. *Plant*

880   *Physiology* 160:2239–2250. DOI: 10.1104/pp.112.207274.

881   Kramer DM., Evans JR. 2011. The importance of energy balance in improving

882   photosynthetic productivity. *Plant physiology* 155:70–8. DOI: 10.1104/pp.110.166652.

883   Li M., Hu D., Liu H. 2014. Photobioreactor with ideal light-dark cycle designed and built

884   from mathematical modeling and CFD simulation. *Ecological Engineering* 73:162–167.

885   DOI: 10.1016/j.ecoleng.2014.09.010.

886   Luengo JM., García BN., Sandoval A., Naharro GN., Olivera ER. 2003. Bioplastics from

887   microorganisms. *Current Opinion in Microbiology* 6:251–260. DOI: 10.1016/S1369-

888   5274(03)00040-7.

889   Luo H-P., Al-Dahhan MH. 2011. Verification and validation of CFD simulations for local

890   flow dynamics in a draft tube airlift bioreactor. *Chemical Engineering Science* 66:907–

891   923. DOI: 10.1016/J.CES.2010.11.038.

892   Mohamed A., Eriksson J., Osiewacz HD., Jansson C. 1993. Differential expression of the

893   psbA genes in the cyanobacterium *Synechocystis* 6803. *MGG Molecular & General*

894   *Genetics* 238:161–168. DOI: 10.1007/BF00279543.

895   Montgomery BL. 2015. Light-dependent governance of cell shape dimensions in

896   cyanobacteria. *Frontiers in Microbiology* 6:1–8. DOI: 10.3389/fmicb.2015.00514.

897   Mulo P., Laakso S., Mäenpää P., Aro E-M. 1998. Stepwise Photoinhibition of Photosystem

898   II. *Plant Physiology* 117:483–490. DOI: 10.1104/pp.117.2.483.

899   Murata N., Takahashi S., Nishiyama Y., Allakhverdiev SI. 2007. Photoinhibition of

900   photosystem II under environmental stress. *Biochimica et Biophysica Acta -*

901   *Bioenergetics* 1767:414–421. DOI: 10.1016/j.bbabio.2006.11.019.

902   Nanjo Y., Mizusawa N., Wada H., Slabas AR., Hayashi H., Nishiyama Y. 2010. Synthesis of

903   fatty acids de novo is required for photosynthetic acclimation of *Synechocystis* sp. PCC

904   6803 to high temperature. *Biochimica et Biophysica Acta - Bioenergetics* 1797:1483–

905   1490. DOI: 10.1016/j.bbabio.2010.03.014.

906   Nedbal L., Trtílek M., Červený J., Komárek O., Pakrasi HB. 2008. A photobioreactor system

907   for precision cultivation of photoautotrophic microorganisms and for high-content

908   analysis of suspension dynamics. *Biotechnology and Bioengineering* 100:902–910. DOI:

909   10.1002/bit.21833.

910   Ooms MD., Graham PJ., Nguyen B., Sargent EH., Sinton D. 2017. Light dilution via

911   wavelength management for efficient high-density photobioreactors. *Biotechnology and*

912   *Bioengineering* 114:1160–1169. DOI: 10.1002/bit.26261.

913   Panda B., Jain P., Sharma L., Mallick N. 2006. Optimization of cultural and nutritional

914   conditions for accumulation of poly-β-hydroxybutyrate in *Synechocystis* sp. PCC 6803.

915   *Bioresource Technology* 97:1296–1301. DOI: 10.1016/J.BIORTECH.2005.05.013.

916   Pattanaik B., Whitaker MJ., Montgomery BL. 2011. Convergence and divergence of the

917   photoregulation of pigmentation and cellular morphology in *Fremyella diplosiphon*.

918   *Plant Signaling & Behavior* 6:2038–2041. DOI: 10.4161/psb.6.12.18239.

919   Alphen V. 2018. Physiological studies to optimize growth of the prototype biosolar cell

920   factory. D. Phil. Thesis, Uviverity of Amsterdam

921   Powles SB. 1984. Photoinhibition of Photosynthesis Induced by Visible Light. *Annual*

922   *Review of Plant Physiology* 35:15–44. DOI: 10.1146/annurev.pp.35.060184.000311.

923   Schuurmans RM., Van Alphen P., Schuurmans JM., Matthijs HCP., Hellingwerf KJ. 2015.

924   Comparison of the photosynthetic yield of cyanobacteria and green algae: Different

925   methods give different answers. *PLoS ONE* 10:1–17. DOI:

926   10.1371/journal.pone.0139061.

927   Singh AK., Bhattacharyya-Pakrasi M., Elvitigala T., Ghosh B., Aurora R., Pakrasi HB. 2009.

928   A systems-level analysis of the effects of light quality on the metabolism of a

929   cyanobacterium. *Plant physiology* 151:1596–608. DOI: 10.1104/pp.109.144824.

930   Singh R., Parihar P., Singh M., Bajguz A., Kumar J., Singh S., Singh VP., Prasad SM. 2017.

931   Uncovering Potential Applications of Cyanobacteria and Algal Metabolites in Biology,

932   Agriculture and Medicine: Current Status and Future Prospects. *Frontiers in*

933   *Microbiology* 8:515. DOI: 10.3389/fmicb.2017.00515.

934   Solimeno A., Samsó R., Uggetti E., Sialve B., Steyer JP., Gabarró A., García J. 2015. New

935   mechanistic model to simulate microalgae growth. *Algal Research* 12:350–358. DOI:

936   10.1016/j.algal.2015.09.008.

937   Stanier RY., Kunisawa R., Mandel M., Cohen-Bazire G. 1971. Purification and properties of

938   unicellular blue-green algae (Order Chroococcales). *Bacteriological reviews* 35:171–

939   205. DOI: 10.1016/j.jbiotec.2013.07.020.

940   Steiger S., Schäfer L., Sandmann G. 1999. High-light-dependent upregulation of carotenoids

941   and their antioxidative properties in the cyanobacterium *Synechocystis* PCC 6803.

942   *Journal of Photochemistry and Photobiology B: Biology* 52:14–18. DOI:

943   10.1016/S1011-1344(99)00094-9.

944   Straka L., Rittmann BE. 2018. Effect of culture density on biomass production and light

945   utilization efficiency of *Synechocystis* sp. PCC 6803. *Biotechnology and Bioengineering*

946   115:507–511. DOI: 10.1002/bit.26479.

947   Theis J., Schroda M. 2016. Revisiting the photosystem II repair cycle. *Plant Signaling and*

948   *Behavior* 11:e1218587. DOI: 10.1080/15592324.2016.1218587.

949   Touloupakis E., Cicchi B., Benavides AMS., Torzillo G. 2016. Effect of high pH on growth

950   of *Synechocystis* sp. PCC 6803 cultures and their contamination by golden algae

951   (Poterioochromonas sp.). *Applied Microbiology and Biotechnology* 100:1333–1341.

952   DOI: 10.1007/s00253-015-7024-0.

953   Trautmann D., Beyer P., Al-Babili S. 2013. The ORF slr0091 of *Synechocystis* sp. PCC6803

954   encodes a high-light induced aldehyde dehydrogenase converting apocarotenals and

955   alkanals. *FEBS Journal* 280:3685–3696. DOI: 10.1111/febs.12361.

956   Triantaphylidès C., Havaux M. 2009. Singlet oxygen in plants: production, detoxification and

957   signaling. *Trends in Plant Science* 14:219–228. DOI: 10.1016/j.tplants.2009.01.008.

958   Tyystjärvi E. 2013. Photoinhibition of Photosystem II*. *International Review of Cell and*

959   *Molecular Biology* 300:243–303. DOI: 10.1016/B978-0-12-405210-9.00007-2.

960   Van Alphen P., Hellingwerf KJ. 2015. Sustained circadian rhythms in continuous light in

961   Synechocystis sp. PCC6803 growing in a well-controlled photobioreactor. *PLoS ONE*

962   10. DOI: 10.1371/journal.pone.0127715.

963   Varman AM., Xiao Y., Pakrasi HB., Tang YJ. 2013. Metabolic engineering of *Synechocystis*

964   sp. Strain PCC 6803 for isobutanol production. *Applied and Environmental*

965   *Microbiology* 79:908–914. DOI: 10.1128/AEM.02827-12.

966   Vass I., Styring S., Hundal T., Koivuniemi a., Aro E., Andersson B. 1992. Reversible and

967   irreversible intermediates during photoinhibition of photosystem II: stable reduced QA

968   species promote chlorophyll triplet formation. *Proceedings of the National Academy of*

969   *Sciences of the United States of America* 89:1408–1412. DOI: 10.1073/pnas.89.4.1408.

970   Vatcheva I., de Jong H., Bernard O., Mars NJI. 2006. Experiment selection for the

971   discrimination of semi-quantitative models of dynamical systems. *Artificial Intelligence*

972   170:472–506. DOI: 10.1016/J.ARTINT.2005.11.001.

973   Vavilin D., Brune DC., Vermaas W. 2005. 15N-labeling to determine chlorophyll synthesis

974   and degradation in *Synechocystis* sp. PCC 6803 strains lacking one or both

975 photosystems. *Biochimica et Biophysica Acta (BBA) - Bioenergetics* 1708:91–101. DOI:

976 10.1016/j.bbabio.2004.12.011.

977 Vavilin D., Vermaas W. 2007. Continuous chlorophyll degradation accompanied by

978 chlorophyllide and phytol reutilization for chlorophyll synthesis in *Synechocystis* sp.

979 PCC 6803. *Biochimica et Biophysica Acta (BBA) - Bioenergetics* 1767:920–929. DOI:

980 10.1016/J.BBABIO.2007.03.010.

981 Vermaas W. 1996. Molecular genetics of the cyanobacterium *Synechocystis* sp. PCC 6803:

982 Principles and possible biotechnology applications. *Journal of Applied Phycology*

983 8:263–273.

984 Wang CY., Fu CC., Liu YC. 2007. Effects of using light-emitting diodes on the cultivation of

985 *Spirulina platensis*. *Biochemical Engineering Journal* 37:21–25. DOI:

986 10.1016/j.bej.2007.03.004.

987 Wilcox DC. 2006. *Turbulence modeling for CFD*. DCW Industries.

988 Wyman M., Fay P. 1986. Underwater Light Climate and the Growth and Pigmentation of

989 Planktonic Blue-Green Algae (Cyanobacteria) II. The Influence of Light Quality.

990 *Proceedings of the Royal Society B: Biological Sciences* 227:381–393. DOI:

991 10.1098/rspb.1986.0028.

992 Xu H., Vavilin D., Funk C., Vermaas W. 2004. Multiple Deletions of Small Cab-like Proteins

993 in the Cyanobacterium *Synechocystis* sp. PCC 6803. *Journal of Biological Chemistry*

994 279:27971–27979. DOI: 10.1074/jbc.M403307200.

995 Yang C., Hua Q., Shimizu K. 2002. Metabolic flux analysis in *Synechocystis* using isotope

996 distribution from 13C-labeled glucose. *Metabolic engineering* 4:202–16.

997 Yao DCI., Brune DC., Vavilin D., Vermaas WFJ. 2012. Photosystem II component lifetimes

998 in the cyanobacterium *Synechocystis* sp. strain PCC 6803: Small Cab-like proteins

999 stabilize biosynthesis intermediates and affect early steps in chlorophyll synthesis.

1000 *Journal of Biological Chemistry* 287:682–692. DOI: 10.1074/jbc.M111.320994.

1001 Yao DCI., Brune DC., Vermaas WFJ. 2012. Lifetimes of photosystem i and II proteins in the

1002 cyanobacterium *Synechocystis* sp. PCC 6803. *FEBS Letters* 586:169–173. DOI:

1003 10.1016/j.febslet.2011.12.010.

1004 Yoshikawa K., Hirasawa T., Ogawa K., Hidaka Y., Nakajima T., Furusawa C., Shimizu H.

1005 2013. Integrated transcriptomic and metabolomic analysis of the central metabolism of

1006 *Synechocystis* sp. PCC 6803 under different trophic conditions. *Biotechnology Journal*

1007 8:571–580. DOI: 10.1002/biot.201200235.

1008 Yu Y., You L., Liu D., Hollinshead W., Tang YJ., Zhang F. 2013. Development of

1009 *Synechocystis* sp. PCC 6803 as a Phototrophic Cell Factory. *Mar. Drugs* 11:2894–2916.

1010 DOI: 10.3390/md11082894.

1011 Zavřel T., Sinetova MA., Búzová D., Literáková P., Červený J. 2015. Characterization of a

1012 model cyanobacterium *Synechocystis* sp: PCC 6803 autotrophic growth in a flat-panel

1013 photobioreactor. *Engineering in Life Sciences* 15:122–132. DOI:

1014 10.1002/elsc.201300165.

1015 Zhang D., Dechatiwongse P., Hellgardt K. 2015. Modelling light transmission,

1016 cyanobacterial growth kinetics and fluid dynamics in a laboratory scale multiphase

1017 photo-bioreactor for biological hydrogen production. *Algal Research* 8:99–107. DOI:

1018 10.1016/j.algal.2015.01.006.

1019 Zhang D., Xiao N., Mahbubani KT., del Rio-Chanona EA., Slater NKH., Vassiliadis VS.

1020 2015. Bioprocess modelling of biohydrogen production by *Rhodopseudomonas*

1021 *palustris*: Model development and effects of operating conditions on hydrogen yield and

1022 glycerol conversion efficiency. *Chemical Engineering Science* 130:68–78. DOI:

1023 10.1016/j.ces.2015.02.045.

1024 Zhou J., Zhu T., Cai Z., Li Y. 2016. From cyanochemicals to cyanofactories: a review and

1025 perspective. *Microbial Cell Factories* 15. DOI: 10.1186/s12934-015-0405-3.

1026

1027

1028

1029 **Figure and table legends**

1030 **Figure 1: Photobioreactor schematic representation.**

1031 **(A)** Body of the flat panel PBR FMT150.2/400 composed of a 390 ml transparent removable

1032 flat vessel. On top of the vessel, a stainless lid accommodates different tubes, connectors and

1033 sensors. The base of the instrument contains a control unit with analogic and digital

1034 electronic circuits. Enlarged the details of the red and blue LEDs installed in the light panel

1035 of the reactor, the densitometer and the fluorometer. **(B)** Red and blue LED spectra of PBR

1036 FMT150.2/400.**(C)** Transmission spectrum of cyanobacterial culture affected by light

1037 absorptions, light scattering. The lines and arrows indicate wavelength of the light sources

1038 present in the flat panel reactor and the detection range of the detector filter. **(D)** 3D modelled

1039 geometry of PBR with modelled domains selection: 1-closing, 2-inoculum, 3-sparger, 4-air,

1040 5-sampling, 6-culture, 7-stirring bar, 8-wall of vessel, 9-base of vessel**.**

1041

1042 **Figure 2: Challenging** *Synechocystis* **by high light intensity revealed its adaptive**

1043 **capacity**.

1044 *Synechocystis* behaviour was assessed by quantifying the growth rate and the relative

1045 concentration of dissolved oxygen in the medium under increasing photon irradiance. The

1046 turbidostat-controlled cultures were grown at constant temperature (30˚C) and pH (8.0) under

1047 orange-red light and acclimated for 24 h at each light intensity. The figure shows

1048 *Synechocystis* ability to fully recover after passing through a complete state of

1049 photoinhibition at 1460 µmol photons m^{-2} s^{-1}. (**A**)Growth rate of *Synechocystis* evaluated at

1050 each light intensity. (**B**) Oxygen released in the medium of the PBR by *Synechocystis*. The

1051 blue dots show the mean values derived from three biological replicates and are accompanied

1052 by their respective standard deviation bars. Data were normalized to the values obtained at 50

1053 µmol photons m^{-2} s^{-1}. The orange triangles show the simulated values according to our PBR

1054 model. In both panels (•) stands for point of recovery, which was set at 200 µmol photons m^{-2}

1055 s^{-1}, and the asterisk (*) indicates that no steady state could be reached in 24 h at this condition

1056 (as shown by the large error bars).

1057

1058 **Figure 3: Recovery of growth of** *Synechocystis* **after high light treatment.**

1059 *Synechocystis* quickly recovers from high light (1460 µmol photons m^{-2} s^{-1}, left side) after

1060 reducing light intensity to a non-photoinhibiting intensity (200 µmol photons m^{-2} s^{-1}, right

1061 side). Dissolved oxygen concentration (red line) and growth rate (black squares, calculated

1062 per turbidostat cycle) are shown. The half-life of this recovery is 3 h.

1063

1064 **Figure 4: Relationship of the cell size and growth rate of *Synechocystis* set at different**

1065 **light intensities.**

1066 The figure displays the relationship between growth rate and cell size at varying light

1067 intensities. Dot colours reflect the incident light intensity, with the green and red colours

1068 corresponding to low values and high values, respectively

1069

1070 **Figure 5. 3D trend of normalized light intensity along YZ slice of the model PBR.**

1071 The calculated light intensity was normalized with respect to the initial incident intensity and

1072 the R_I trend is performed along six YZ planes for three different incident light intensities, I_{inc}.

1073 (**A**) 50 µmol photons m^{-2} s^{-1}. (**B**) 300 µmol photons m^{-2} s^{-1}. (**C**) 950 µmol photons m^{-2} s^{-1}.

1074

1075 **Figure 6. 2D trend of normalized light intensity along XZ slice of the model PBR.**

1076 The calculated light intensity was normalized with respect to the initial incident intensity and

1077 the R_I trend is performed along three XZ planes for three different incident light intensities,

1078 I_{inc} (**A**) 50 µmol photons m^{-2} s^{-1}. (**B**) 300 µmol photons m^{-2} s^{-1}. (**C**) 950 µmol photons m^{-2} s^{-1}.

1079

1080 **Table 1. Cell size and dry cell weight of *Synechocystis* grown under increasing light**

1081 **intensities**.

1082 The turbidostat-controlled cultures were grown at constant temperature (30˚C) and pH (8.0)

1083 under orange-red light and acclimated for 24 h at each light intensity. The values are mean

1084 and standard deviation derived from three biological replicates. (*) Point of recovery at 200

1085 µmol photons m^{-2} s^{-1}.

1086 **Table 2 Comparison of the efficiency of photosynthesis in terms of moles of photons**

1087 **required for biomass production in *Synechocystis* calculated from growth simulations in**

1088 **a 380 ml vessel of the PBR upon acclimation for 24 h at 50, 200, 300 ,500, 800and950**

1089 **µmol photons m^{-2}s^{-1} of orange-red light.**

1090   Shown are: I_{in} (μmol photons m^{-2}s^{-1}), light intensity available to the PBR domains; μ h^{-1},

1091   growth rate per hour; g DW L^{-1}, biomass density in gram dry weight per liter; g DW /mol

1092   photons, growth yield in mol photons absorbed per gram biomass.

1093

1094

1095   **Supporting Informations**

1096

1097   **Figure S1. 3D slice trend of dispersed phase.**

1098   The dispersed phase mixture of CO_2 and N_2 is plotted at 24 h and for incident light intensitiy,

1099 I_{inc}, equal to 300 μmol photons m^{-2} s$^-$1

1100

1101   **Figure S2. 3D visualization of three cut planes.**

1102   The red planes represent the surface in which the R_I is plotted in Fig.6

1103

1104   **Table S1. Model equations.**

1105   The mathematical equations implemented in the software are listed and subdivided by the

1106   phenomena described, with the selection of computing domains.**S2 Table. Estimation of Chl**

1107   ***a* content in *Synechocystis* cells acclimated to different light intensities.**

1108   Measurement by the PBR of the OD_{680}/OD_{720} ratio, indicative of Chl *a* cellular content. The

1109   turbidostat-controlled cultures were grown in red-orange light under constant temperature

1110   (30˚C) and pH (8.0). (*) Point of recovery at 200 μmol photons m^{-2} s^{-1}.

1111

1112   **Table S3. Geometry of photobioreactor.**

1113

1114   **Table S4. Boundary and operative conditions.**

1115

1116   **Table S5. Comparison of the efficiency of photosynthesis in terms of moles of photons**

1117   **required for biomass production in *Synechocystis* calculated from growth simulations in**

1118   **a 380 ml vessel of the PBR upon acclimation for 24 h at 50, 200, 300 , 500 , 800 and 950**

1119   **μmol photons m^{-2}s^{-1} of orange-red light.**

1120

Figure 1

Photobioreactor schematic representation.
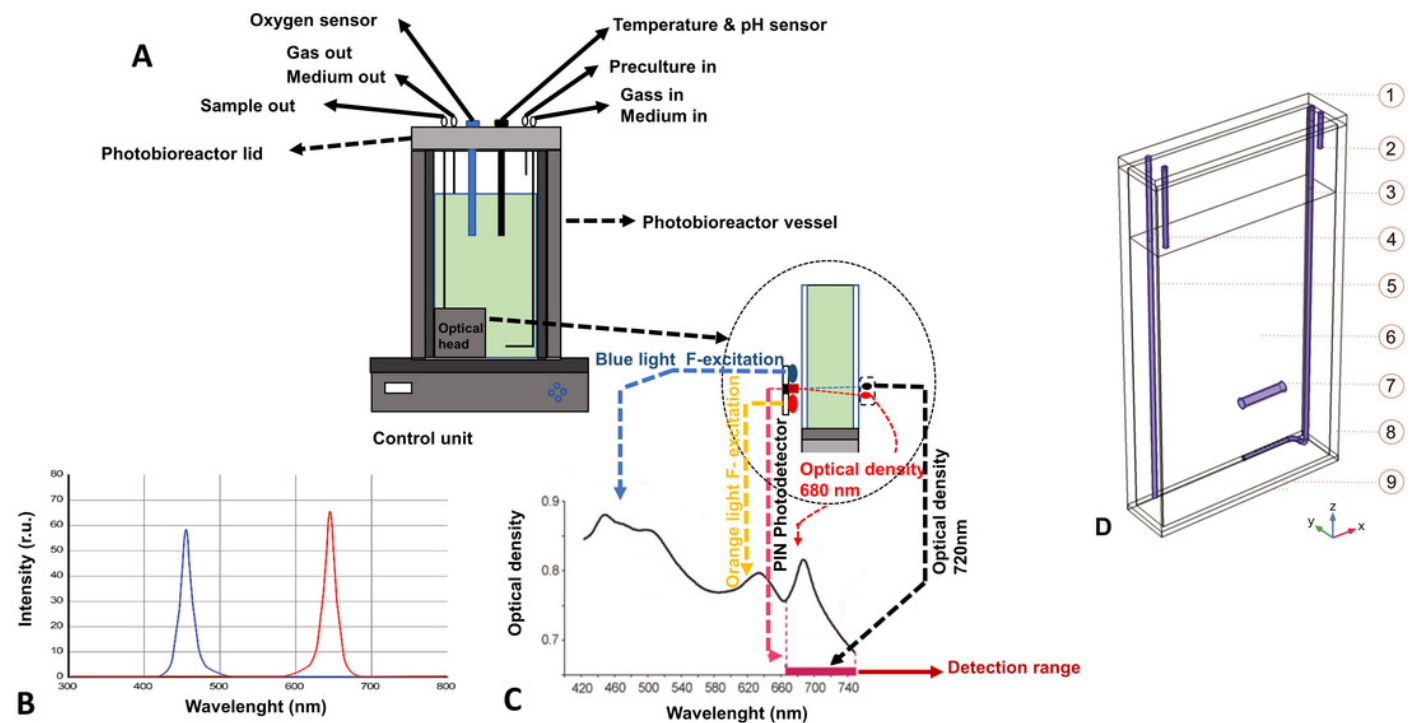
Figure 2

Challanging Synechocystis by high light intensity revealed its adaptive capacity.

Synechocystis behaviour was assessed by quantifying the growth rate and the relative concentration of dissolved oxygen in the medium under increasing photon irradiance. The turbidostat-controlled cultures were grown at constant temperature (30°C) and pH (8.0) under orange-red light and acclimated for 24 h at each light intensity. The figure shows *Synechocystis* ability to fully recover after passing through a complete state of photoinhibition at 1460 μmol photons m^{-2} s^{-1}. (**A**) Growth rate of *Synechocystis* evaluated at each light intensity. (**B)** Oxygen released in the medium of the PBR by *Synechocystis*. The blue dots show the mean values derived from three biological replicates and are accompanied by their respective standard deviation bars. Data were normalized to the values obtained at 50 μmol photons m^{-2} s^{-1}. The orange triangles show the simulated values according to our PBR model. In both panels (•) stands for point of recovery, which was set at 200 μmol photons m^{-2} s^{-1}, and the asterisk (*) indicates that no steady state could be reached in 24 h at this condition (as shown by the large error bars).
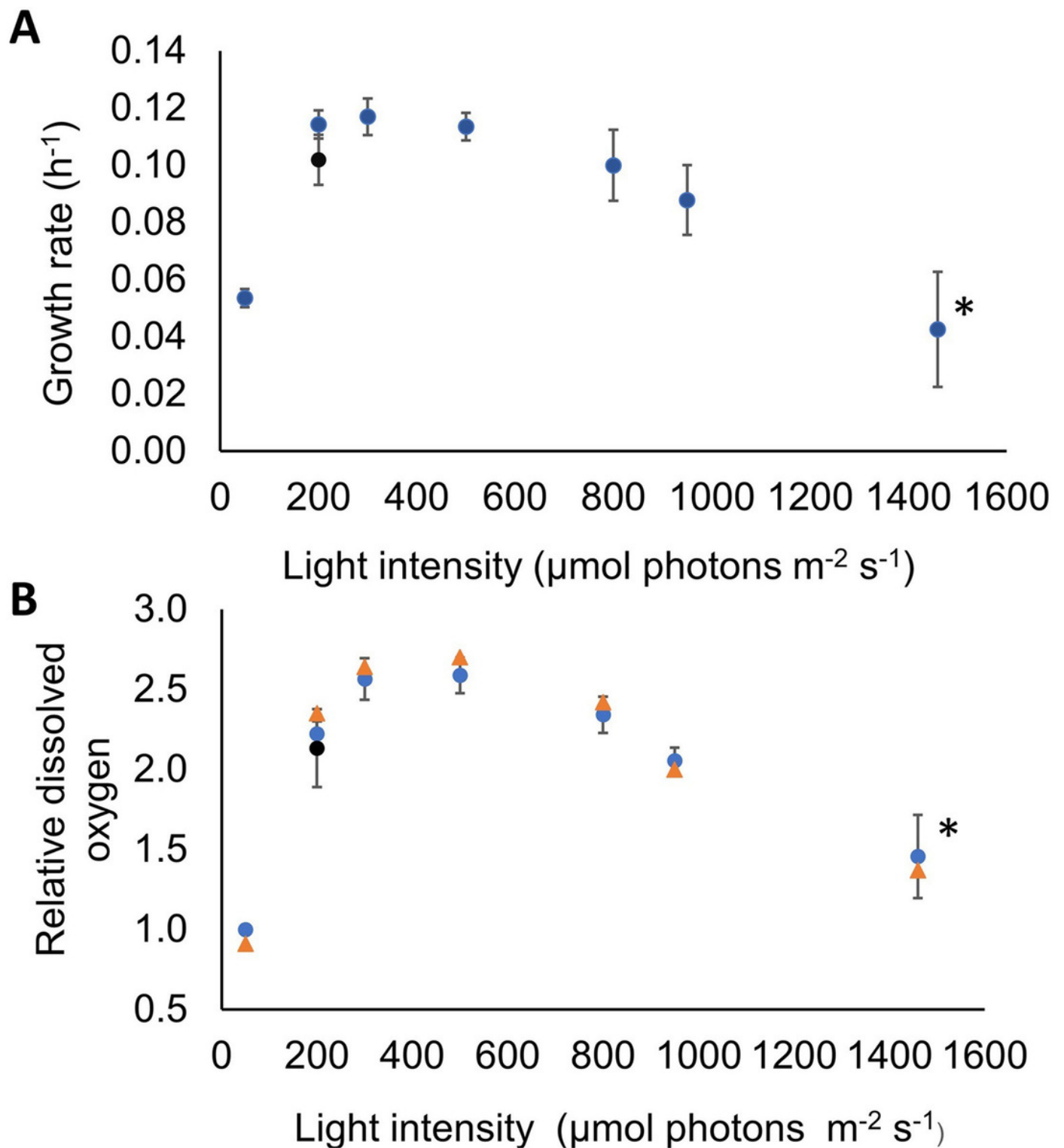
Figure 3

Recovery of growth rate of Synechocystis after high light treatment.
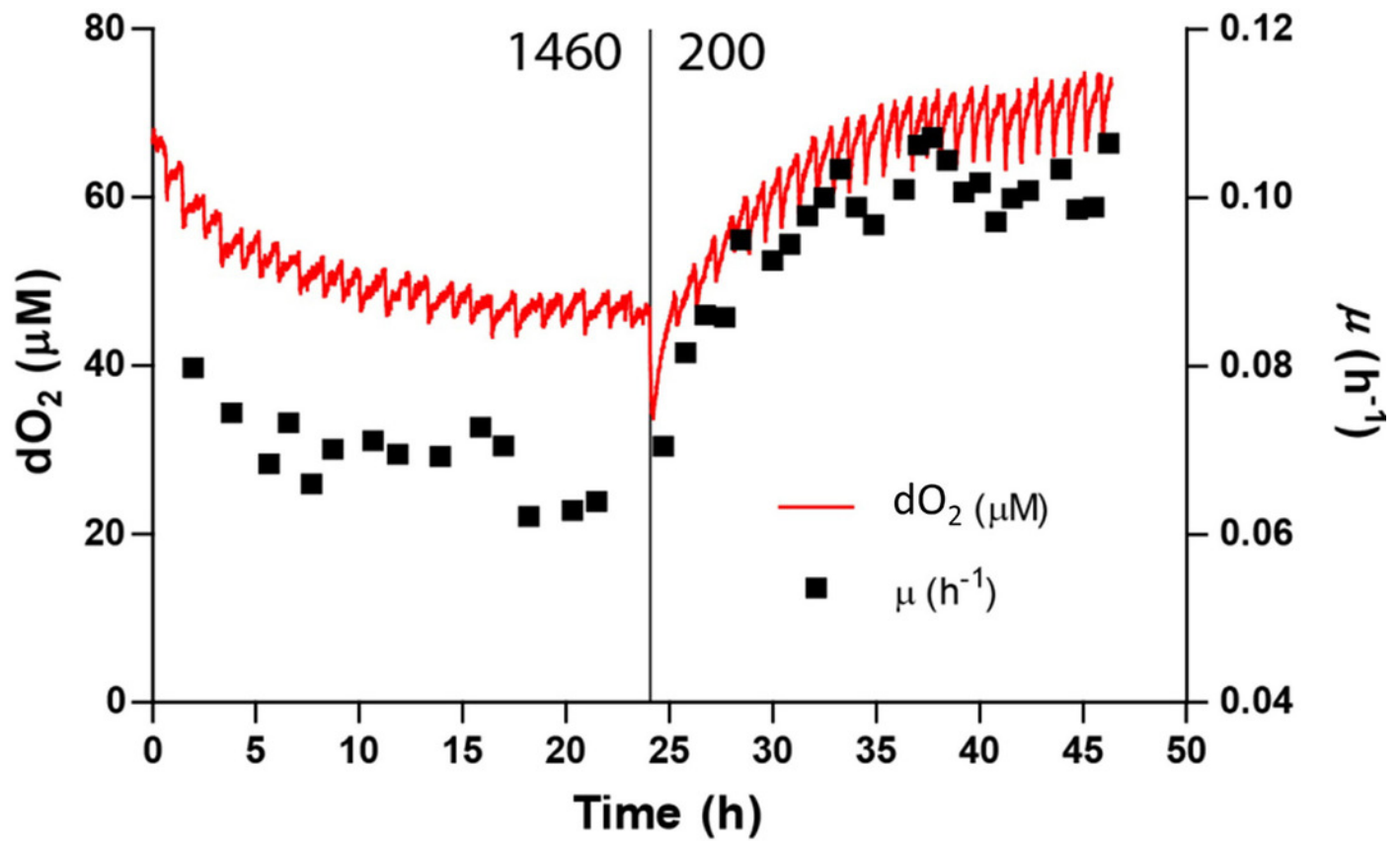
Figure 4

Relationship of the cell size and growth rate of Synechocystis set at different light intensities.
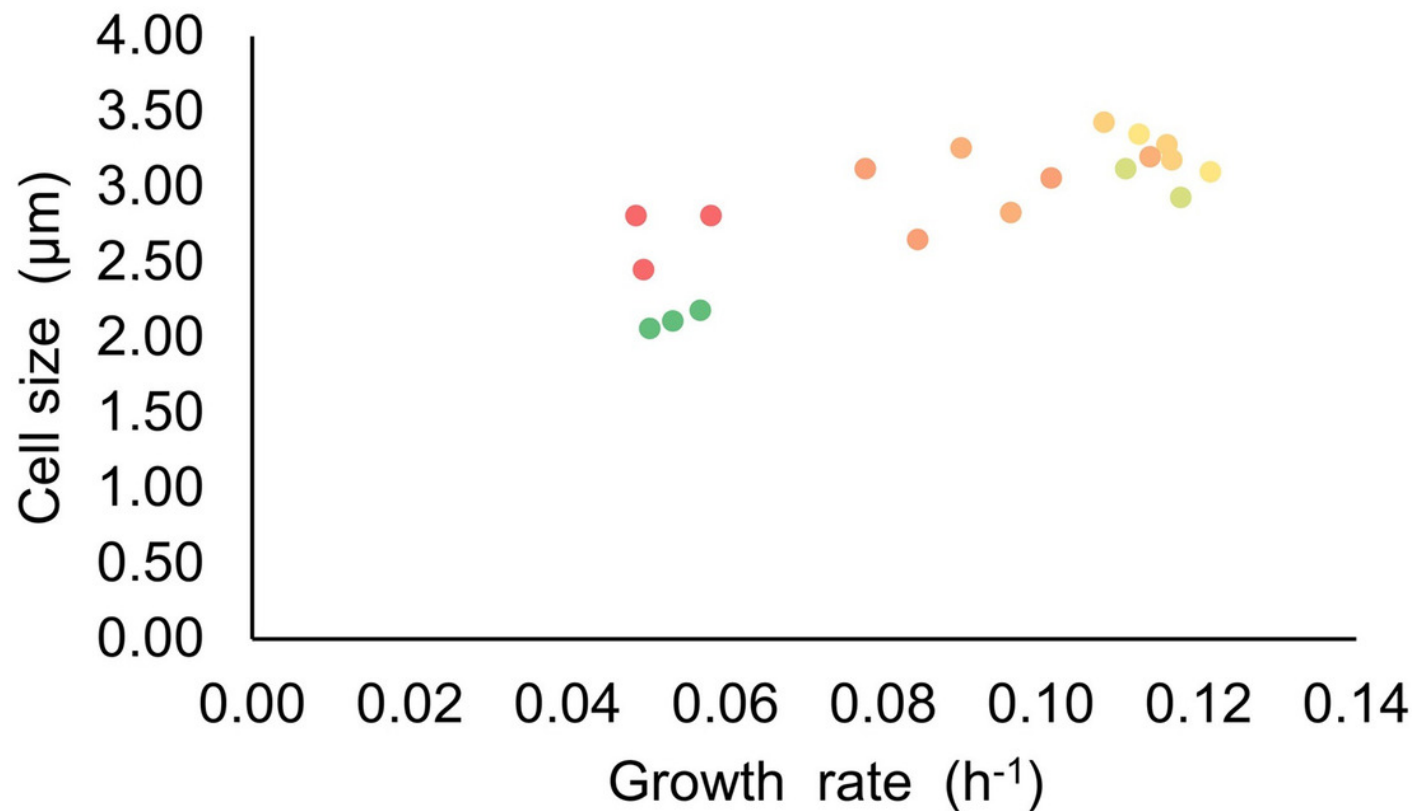
Figure 5

3D trend of normalized light intensity along yz slices of the model PBR.

The calculated light intensity was normalized with respect to the initial incident intensity and the RI trend is performed along six YZ planes for three different incident light intensities, Iinc. (A) 50 µmol photons m-2 s-1. (B) 300 µmol photons m-2 s-1. (C) 950 µmol photons m-2 s-1.
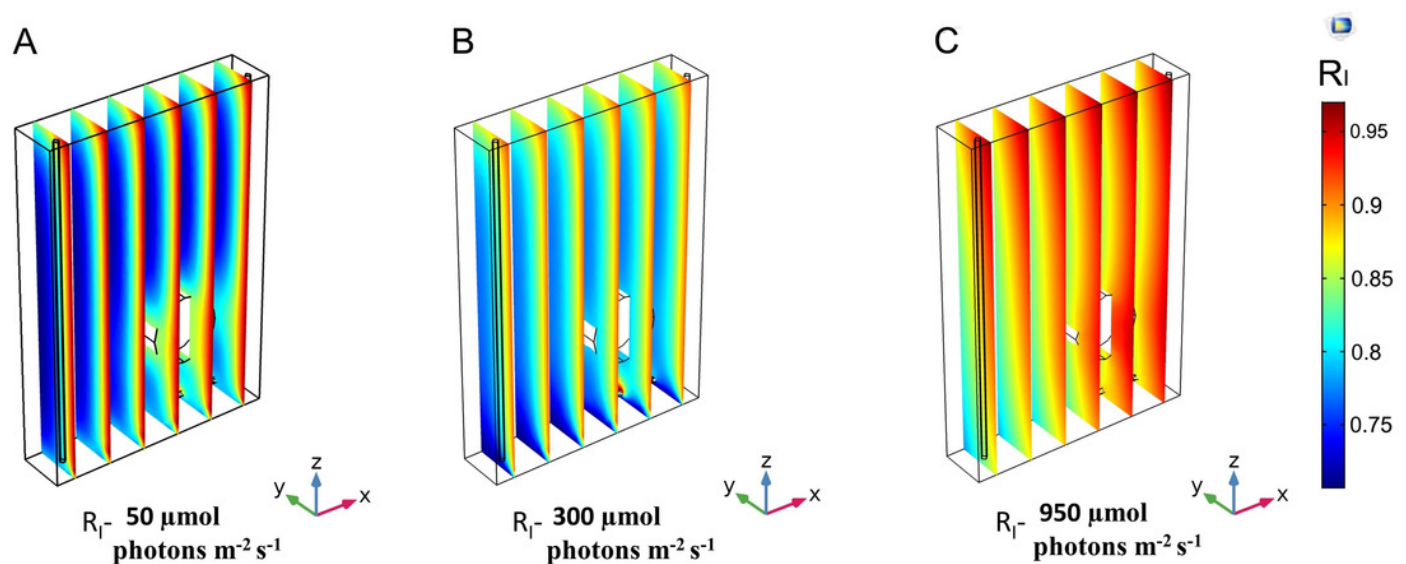
Figure 6

2D trend of normalized light intensity along the xz slices of the model PBR.
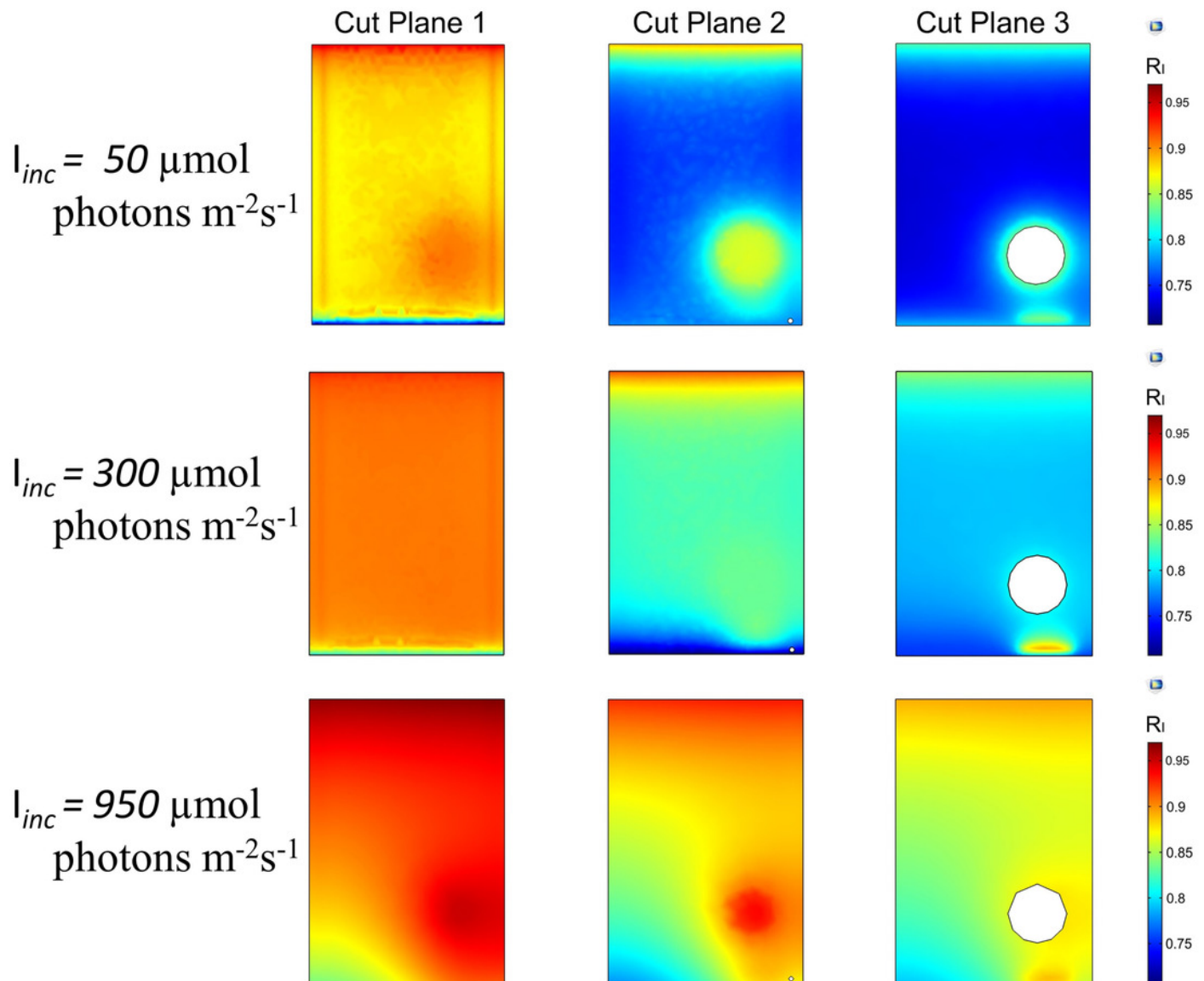
Cell size and dry cell weight of Synechocystis grown under increasing light intensities.

1 **Table 1**

Light intensity (μmol photons m^{-2} s^{-1})	Cell size (μm)	Dry cell weight (g OD$_{730}$$^{-1}$* L^{-1})
50	2.11 ± 0.06	0.145 ± 0.001
200	3.02 ± 0.13	0.140 ± 0.021
300	3.22 ± 0.18	0.145 ± 0.005
500	3.29 ± 0.13	0.147 ± 0.003
800	3.09 ± 0.23	0.152 ± 0.004
950	2.94 ± 0.26	0.153 ± 0.000
1460	2.69 ± 0.21	0.158 ± 0.021
200*	3.03 ± 0.01	0.150 ± 0.003

Comparison of the efficiency of photosynthesis

Comparison of the efficiency of photosynthesis in terms of moles of photons required for biomass production in Synechocystis calculated from growth simulations in a 380 ml vessel of the PBR upon acclimation for 24 h at 50, 200, 300, 500, 800 and 950 μmol photons $m^{-2}s^{-1}$ of orange-red light. Shown are: I_{in} (μmol photons $m^{-2}s^{-1}$), light intensity available to the PBR domains; μ h^{-1}, growth rate per hour; g DW L^{-1} , biomass density in gram dry weight per liter; g DW /mol photons, growth yield in mol photons absorbed per gram biomass.

1 **Table 2.**

I_{in} (µmol photons m^{-2}s^{-1})	Vol L	µ h^{-1}	gDW L^{-1}	mol photons g DW^{-1}	efficiency
50	0,377	0,054	0,145	0,37	2,70
200	0,377	0,110	0,140	0,61	1,64
300	0,377	0,117	0,145	0,75	1,33
500	0,377	0,110	0,147	1,11	0,90
800	0,377	0,104	0,152	1,68	0,60
950	0,377	0,088	0,153	2,10	0,48

4